BNL-111834-2016-JA

Spontaneous and strong multi-layer graphene n-doping on soda-lime glass and its application in graphene-semiconductor junctions

D. M. N. M. Dissanayake[1*], A. Ashraf [1,2], D. Dwyer[3], K. Kisslinger[4], L. Zhang[4], Y. Pang[1,2], H. Efstathiadis[3] and M. D. Eisaman[1,2,5*]

[1]Sustainable Energy Technologies Department, Brookhaven National Laboratory, Upton, NY 11973.

[2]Department of Physics and Astronomy, Stony Brook University, Stony Brook, NY 11794.

[3]Colleges of Nanoscale Science and Engineering (CNSE) at SUNY Polytechnic Institute, Albany, NY 12203.

[4]Center for Functional Nanomaterials, Brookhaven National Laboratory, Upton, NY 11973.

[5]Department of Electrical & Computer Engineering, Stony Brook University, Stony Brook, NY 11794.

*Correspondence to: meisaman@bnl.gov, nanditha.dissanayake@gmail.com

Scalable and low-cost doping of graphene could improve technologies in a wide range of fields such as microelectronics, optoelectronics, and energy storage. While achieving strong p-doping is relatively straightforward, non-electrostatic approaches to n-dope graphene, such as chemical doping, have yielded electron densities of 9.5×10^{12} *e*/cm^2 or below. Furthermore, chemical doping is susceptible to degradation and can adversely affect intrinsic graphene's properties. Here we demonstrate strong (1.33×10^{13} *e*/cm^2), robust, and spontaneous graphene n-doping on a soda-lime-glass substrate via surface-transfer doping from Na without any external chemical, high-temperature, or vacuum processes. Remarkably, the n-doping reaches 2.11×10^{13} *e*/cm^2 when graphene is transferred onto a p-type copper indium gallium diselenide (CIGS) semiconductor that itself has been deposited onto soda-lime-glass, via surface-transfer doping from Na atoms that diffuse to the CIGS surface. Using this effect, we demonstrate an n-graphene/p-semiconductor Schottky junction with ideality factor of 1.21 and strong photo-response. The ability to achieve

strong and persistent graphene n-doping on low-cost, industry-standard materials paves the way toward an entirely new class of graphene-based devices such as photodetectors, photovoltaics, sensors, batteries, and supercapacitors.

The benefit of using of chemical-vapor-deposited (CVD) graphene as a passive transparent electrode[1,2] is well recognized, but its potential to be paired with a semiconductor and play an active role as part of an electronic junction remains a very active field of research[3-7]. To enable more control in fabricating active graphene-semiconductor junctions, pristine CVD graphene must be doped p-type or n-type, since unlike epitaxial graphene[8], it is not doped upon growth. Electrostatic[4-6] and chemical doping[7] have resulted in Schottky diodes between p-doped graphene and n-type silicon. However, unlike p-doping, which occurs even naturally for graphene exposed to atmospheric water molecules[9], persistent graphene n-doping with high electron density that is resistant to degradation has been more difficult to achieve. To this end, nitrogen based precursors during growth[10] as well as amines[11,12] and transition/alkali metals[13-17] after growth have been explored. Although these approaches have shown promise in highly controlled experimental settings, all existing persistent n-doping techniques[10-17] fail to achieve the strength (more than 9.5×10^{12} e/cm^2 (Ref. 11)) , robustness, and scalability ultimately required for most applications[1,2]. Previous reports have shown that adsorbed alkali-metal atoms cause strong n-doping in graphene, but challenges remain, such as the reactivity of alkali metals and the lack of a scalable process[15]. We demonstrate that an alkali metal (Na) embedded in inert, industrial-grade (~8% Na_2O), low-cost soda-lime glass (SLG) overcomes these challenges and strongly n-dopes graphene (1.33×10^{13} e/cm^{-2}, see Fig. S1 in the Supplementary Information for comparison to the n-doping strength achieved in Refs.10-15) via surface-transfer doping from Na, upon transfer of CVD-grown graphene onto the SLG. Initial tests show that the doping

strength does not degrade when the devices are left in air for several weeks, which is already superior to previously demonstrated methods. The persistence of the doping achieved with this technique (that is, the resistance to degradation) is due to the effectively inexhaustible reservoir of Na in the SLG, in contrast to chemical doping where the doping strength degrades due to the reactivity or evaporation of the finite amount of externally introduced dopants[10-12].

A field-effect transistor (FET) with multi-layer graphene (GR) transferred onto SLG (8% Na_2O) was characterized to obtain a plot of conductance (G) (maximum normalized to one) vs. gate-voltage (V_G) (Fig. 1a). The minimum G value (i.e., Dirac point) is seen at -67V, indicating n-doping of 1.33×10^{13} e/cm^{-2} and a Fermi energy shift (ΔE_F) of +426meV. Photoelectron spectroscopy and secondary ion mass spectrometry (SIMS) of Na in the SLG (supplementary Figs. 4 and 5) indicate a Na surface density (ρ_{Na}) of $\rho_{Na} = 1.15 \pm 0.05 \times 10^{14}$ cm^{-2} at the surface adjacent to graphene; similar densities of alkali metals on graphene are known to induce strong n-doping via electron transfer from the metal atoms to graphene[16,17]. Density functional theory (DFT) calculations (Supplementary section 10) that assume a Na monolayer on graphene (with $\rho_{Na} = 7.6 \times 10^{14} cm^{-2}$ − close to the measured surface-density of Na on SLG), show n-doping with ΔE_F = +474meV (Fig. 1b), in close agreement with the experimental measurements (ΔE_F = +426meV). The measured charge-transfer rate of 0.11*e* per-Na-atom is also in agreement with literature values of 0.1*e*-0.2*e* [13,17]. As a control experiment, the transconductance of a graphene FET on a low-Na (<1% Na_2O) borosilicate-glass (BSG) substrate shows a Dirac point at V_G ~0V (inset Fig. 1a), indicating no doping and attributable to the lower ρ_{Na} (~$2.30 \pm 0.3 \times 10^{13}$ cm^{-2}, Fig. S5) of BSG compared to SLG. These measurements confirm that the strong graphene n-doping on SLG is caused by charge transfer from the high density of Na near the surface.

Next, to test if graphene/p-type semiconductor/SLG substrates result in n-doping of graphene via Na diffusion through the semiconductor, and the corresponding formation of a p-n junction, we deposited p-type CIGS onto the Mo-side of a Na-rich SLG substrate coated with 330nm of Mo, and then transferred graphene onto the CIGS surface. CIGS/Mo/SLG was chosen because it is a standard substrate used in the solar industry, and so our measurements will help determine the feasibility and versatility of this doping method in real-world applications. SLG substrates are commonly used because Na in CIGS is known to improve solar cell performance[18,19]. During co-evaporation of CIGS on to Mo/SLG above 550 ^{o}C (evaporated Mo layer on SLG serves as a contact), Na diffuses from the SLG into the CIGS along the grain-boundaries seeking oxygen for an octahedral co-ordination[20], ultimately forming Na_2CO_3, $NaSeO_3$, or NaOH at the CIGS/air surface[18,21]. Figure 1c indicates that the Na concentration in CIGS increases rapidly near the CIGS/air surface, reaching a value of ρ_{Na} =4.18x10^{13} cm^{-2} at the surface. In contrast, the CIGS/air surface ρ_{Na} in CIGS/Mo/BSG is nearly two orders of magnitude lower (ρ_{Na} =6.16x10^{11} cm^{-2}).

The HR-TEM in Fig. 1d shows that the graphene on top of the CIGS/Mo/SLG substrate is multi-layer graphene with 5-layers and an interplanar spacing of 340pm, in agreement with previous reports for pristine graphene (335pm)[22]. Raman spectroscopy (Fig.1e) shows the primary CIGS peak[23] at 177 cm^{-1}, along with the graphene G peak at 1585 cm^{-1} and the 2D peak[24] at 2665 cm^{-1}; the graphene D peak[24] at 1350 cm^{-1} is negligible, indicating minimal damage during transfer to the rough CIGS surface (Fig. S2). Energy dispersive spectroscopy (EDS) (Fig. 1f) reveals that Na is distributed uniformly (top-panel) in-plane along the GR/CIGS interface, making electronic interactions between the Na and graphene extremely likely (Fig. 1g). We note that by using a configuration in which the Na host (not necessarily SLG) is in direct

contact with graphene (Na-host/graphene/semiconductor), this approach can be used to form n-graphene/p-semiconductor junctions for a wide range of p-type semiconductors.

The doping effects and junction properties of graphene on CIGS/Mo/SLG (and on CIGS/Mo/BSG) are investigated using the four-terminal device in Fig. 2a. Fig. 2b shows an SEM top-view and the inset shows a TEM cross-section. Fig. 2c shows the conductance (normalized) vs.V_G and the ΔE_F of each device (schematic on right). For GR/CIGS/Mo/SLG (red-curve), the conductance minimum V_G (Dirac point) exceeds the measurement limit and is estimated via extrapolation to be V_G = -106V (Fig. S8), confirming strong n-doping (2.11×10^{13} e/cm^{-2}) with ΔE_F = +536meV, surpassing the ΔE_F for graphene on neat SLG (green-curve). This strong n-doping results from the high Na density that diffuses through CIGS and concentrates at the CIGS/air surface (ρ_{Na} =4.18×10^{13} cm^{-2}, Fig. S7). This conclusion is supported by the fact that graphene on CIGS/Mo/BSG (yellow-curve) with CIGS/air surface ρ_{Na} =6.16×10^{11} cm^{-2} (Fig. S7) is not doped, similar to GR/BSG (cyan-curve). Furthermore, ΔE_F = +536meV of GR/CIGS/Mo/SLG agrees with the potential-shift ($\Delta\Phi$) (+698meV) due to the Na-ion dipole interaction on graphene, as calculated using Helmholtz equation (see Supplementary Information, Section 6)[25]. Comparatively, the calculated shift for GR/CIGS/Mo/BSG with ρ_{Na} = 6.16×10^{11} cm^{-2} is $\Delta\Phi$ ~10meV, explaining the lack of n-doping. Interestingly, the electron transfer rate from Na to graphene in GR/CIGS/Mo/SLG (0.50*e* per-Na-atom), is higher than in GR/SLG (0.11*e* per-Na-atom), which we attribute to ionization-rate differences of the Na species on the CIGS and SLG surfaces.

Fig. 2d is the current-voltage (I-V) curve between graphene-Mo contacts in the dark (dashed), and 11.14mW cm^{-2} white light (solid), with (red) and without (blue) the Al_2O_3 gate-dielectric (Fig. 2a). These measurements show non-linear diode-behavior with a photocurrent

response, with much higher performance when the Al_2O_3 top layer is present. Relative to the measurements without the Al_2O_3 top-layer, the reverse saturation current density (J_0) with Al_2O_3 is reduced by 10^4 to 0.36 nA/cm^2 (Fig. S10), the photocurrent is enhanced by a factor of 650 at -10mV, and the ideality factor becomes as low as 1.29. Fig. 2c shows that a control GR/SiO_2/p-Si FET without the Al_2O_3 dielectric (dashed blue curve) has a Dirac point beyond V_G =+100V, indicating strong p-doping; a GR/SiO_2/p-Si FET with the Al_2O_3 dielectric (Fig. 2c, solid blue curve) shows much less p-doping, with a Dirac point near V_G ~ 20V. These measurements demonstrate that the Al_2O_3 dielectric shields the graphene from p-dopants in ambient air, resulting in an enhanced Schottky barrier (Φ_b) and built-in field.

Fig. 2e shows I-V curves of GR/CIGS/Mo/SLG at different V_G, where J_0 is reduced as V_G is increased from -100V to 50V. Plotting $\ln(J_O)$ vs. $(|V_G + \Delta V_F|)^{1/2}$, we obtain Φ_b = 0.29eV (Supplementary Information, Section 8). The photocurrent at zero-bias increases as graphene is n-doped further by increasingly positive V_G (Fig. 2f), which we attribute to the concomitant increase in the built-in field. Moreover, under 1000W m^{-2} illumination at V_G=0, the photocurrent is 13.6 mA/cm^2, yielding a power conversion efficiency of ~1% ; this represents the first demonstration of n-graphene/p-CIGS photovoltaic behavior. The lowest ideality factor obtained was 1.21 (Fig. S11), indicating negligible recombination in the space-charge region[26].

The behavior of J_0 vs. temperature (T) is modeled assuming Landauer transport[5] in the GR/CIGS/Mo/SLG (Fig. 3a) giving Φ_b = 0.13eV. Assuming ideal Schottky-diode behavior, $\ln(J_o/T^2)$ vs. *1/T* (inset to Fig. 3a) yields Φ_b = 0.11eV, with a constant Richardson coefficient of 1.18x10^{-6} mAcm^{-2}K^{-2}. As is discussed below, this range for Φ_b (0.11eV – 0.29 eV) is lower than expected, which we believe is due to surface defects and surface sodium doping of CIGS that lowers the surface ionization potential of CIGS relative to the bulk.

The barrier height (Φ_b) is equal to the ionization potential of the CIGS semiconductor (IP_{CIGS}) minus the work function of graphene (Φ_G), and represents the barrier that a hole in the valence band of CIGS must overcome to reach the graphene interface and recombine with an electron there. The activation energy (E_a), on the other hand, represents the characteristic energy that governs the rate of minority carrier (electron) excitation into the conduction band of the p-type semiconductor CIGS. In an intrinsic semiconductor, E_a is equal to half the bandgap, and for a doped p-type semiconductor like CIGS, its value should be close to the bandgap energy, since in this case the Fermi level is close to the valence band.

While fitting the J_0 *vs.* T data to the Schottky barrier model allows us to determine Φ_b, fitting this same data to the modified-Arrhenius/activation-energy model (Eqs. (S11), (S12), and Fig. 3b) allows us to determine a value for E_a, which will indicate whether the recombination is predominantly bulk or interfacial. The ideality factor n is expected to become temperature dependent in the presence of tunneling. The measured I-V data is used to determine n as a function of temperature and this is directly incorporated into Eq. (S11), which allows us to separate the effects of E_a and n on the reverse saturation current density J_0. Fig. 3b shows a modified Arrhenius-plot of $n \ln(J_o)$ vs. $1/T$ (where n is the ideality factor), yielding an activation energy (E_a) of 0.96 eV, which indicates dominant interfacial recombination since it is less than the CIGS bandgap of 1.15eV (Ref. 26). We have demonstrated that this interfacial recombination can be reduced using a very thin (4nm) TiO_2 blocking layer between graphene and CIGS, thereby improving V_{oc} from 0.23 V to 0.49 V (Fig. S14). The space-charge width (W_d) of the diode is measured to be 190nm using C-V measurements (Fig. 3c). The approximate band structure of the Schottky diode is given in Fig. 3d. The difference between the CIGS ionization-potential (IP_{CIGS} = 5.65eV (Ref. 27)), and graphene work function 4.69 eV (Ref. 28) modified by

the image-potential correction (0.15eV), gives a theoretical Φ_b^T = 0.81eV. Due to defects[29] and Na surface density[30], IP_{CIGS} is ~0.5eV lower, yielding Φ_b^T = 0.31eV, which is much closer to the measured range of Φ_b = 0.11eV – 0.29eV. It is worth noting that even though the best-fit range of Φ_b (0.11 eV – 0.29 eV) is much less than the best-fit value of E_a (0.96 eV), both models yield good fits to the same J_0 *vs.* T data due to the inclusion of the temperature-dependent n in the activation-energy model.

In conclusion, we have demonstrated strong (1.33×10^{13} e/cm^{-2}, corresponding to a Fermi energy shift of +426meV.), robust, and spontaneous n-doping of graphene on the surface of a low-cost industrial-grade soda-lime-glass substrate via surface-transfer doping from the Na. By leveraging the Na diffusion through a p-type CIGS semiconductor deposited onto the soda-lime glass, we applied this method to the formation of a graphene(n)/semiconductor(p) Schottky diode with even stronger graphene n-doping (2.11×10^{13} e/cm^{-2}, corresponding to a Fermi energy shift of +536meV) than was achieved on bare glass. This method of n-doping does not require any high-temperature annealing steps, and should be compatible with a wide range of semiconductor/substrate systems. The junction properties, such as Schottky barrier height and interfacial recombination rate, can be controlled by tuning the doping strength via the thickness of a few-nm dielectric layer such as TiO_2 or Al_2O_3. Advantages of this technique include the lack of external chemicals whose doping strength decays over time, the ability to achieve strong and persistent n-doping of graphene that is placed on top of a p-doped semiconductor, the ability to n-dope graphene on a wide range of p-doped semiconductors via the use of a Na host that is in direct contact with the graphene layer, and the ability to control the strength of the doping via the use of a spacer layer (e.g., TiO_2) between the Na host and the graphene layer. Disadvantages include the possible restriction to p-doped semiconductors that are not too strongly affected by

the Na diffusion from the Na host to the graphene layer, in the case where the semiconductor lies between the Na host and the graphene layer.

Strong, robust, and tunable graphene doping opens the door for the practical realization of many envisioned applications of graphene such as touch screens and organic light-emitting diodes[1], where the reduction of sheet resistance is crucial to future success, and a broad array of other applications where strong and tunable n-doping is important, such as microelectronics, photodetectors, photovoltaics, electrochemical energy storage, and sensors[2].

Methods

CIGS deposition on Mo/SLG: Given in Supplementary Information, Section 2.

Device Fabrication: Supplementary Fig. S3 shows a schematic of the graphene/CIGS device fabrication process. In order to make our GR/CIGS devices, 450 nm of SiO_2 is first deposited on top of the CIGS/Mo/SLG (BSG) substrates via plasma-enhanced chemical vapor deposition (PECVD) at 160 ^oC at 1.6 nm/s rate. Next, 1x1 μm^2 - 500x500 μm^2 regions were patterned on the PECVD SiO_2 either using optical lithography (or ebeam lithography) techniques depending on the feature size. E-beam was performed using the E-beam lithography JEOL JBX-6300FS system on E-beam resist positive resist ZEP520A (spun at 2000 rpm for 40 sec annealed at 180 ^oC for 3 minutes) by exposing with a dose of 400 $\mu C/cm^2$ at 100 keV and developed with hexylacetate for 90 sec. In optical lithography, the tool MA6 Mask aligner was used with positive optical resist S1811spun at 4000 rpm for 45 sec annealed at 110 ^oC for 1 minute, and developed with MIF 312 3:2 with DI water for 1 minute. These patterned regions were then etched via Reactive Ion Etching (RIE) (Oxford Plasmalab 100 ICP etcher) using a mixture of (CHF_3 and Ar) at 15 nm/min, until the CIGS was exposed. Commercially obtained CVD graphene on Cu foil (Graphene Platform) was then transferred from the Cu substrates to the SiO_2/CIGS/Mo glass substrates. The graphene transfer was done by coating the graphene side of the graphene/Cu foils with PMMA (10% w/w in chlorobenzene spun at 3000 rpm for 1min sec and annealed at 140 ^oC per 1 min), oxygen plasma etching (March Plasma Etcher, 20 W, 100 mT for 20 sec) the opposite side, and etching the Cu using ammonium persulfate (0.1 M) solution overnight. As the Cu is etched away, the graphene/PMMA film floats on the etchant and it is washed in de-ionized water (> 18 MΩ resistivity using a Millipore DI system) and it then transferred, graphene-side down, onto the pattered CIGS/Mo/SLG or other control substrates

such as neat SLG or BSG substrate. Afterwards, graphene transferred substrates are annealed at 100 ^{o}C for 30 minutes in a vacuum oven to remove water, and are subsequently annealed at 200 ^{o}C for 15 minutes to soften the PMMA and promote conformal adhesion onto substrates. It is found that the 200 ^{o}C annealing step is extremely critical in getting highly uniform, wrinkle- and damage-free graphene films on the rough surfaces of CIGS and SiO2 substrates. Afterwards, the PMMA is removed from the graphene by immersing in acetone overnight and the substrate is further annealed in a Rapid Thermal Annealer at 375 ^{o}C in Ar(96%): H_2(4%) forming gas for 15 minutes for complete PMMA removal. Next, the graphene is etched following optical (ebeam) lithographic patterning using oxygen plasma etch. (March plasma, 100 W and 100 mT for 1 minutes or Oxford Plasma Lab DRIE at 20 ^{o}C for 20 seconds in O_2) using a negative tone resist mask (E-beam lithography uses ma-N 2403, spun at 2000 rpm for 30 sec exposed at 200 $\mu C/cm^2$ dose for 100 keV for electron beam and developed using ma-D 532 negative tone developer for 1 minute, Optical lithography uses maN-1410 negative resist spun at 3000 rpm for 30 seconds exposed and developed in ma-D 533 for 1 minute). After etching the graphene, source-drain electrical contacts (Au (30 nm)/Cr (5 nm)) are deposited using ebeam evaporation after optical (ebeam) lithography patterning. Next, a 200nm top gate-dielectric layer (Al_2O_3) is blanket deposited on GR/CIGS/Mo/SLG(BSG) or GR/SLG(BSG) substrates via Atomic Layer Deposition at 1 Å/cycle using (Tri Methyl Aluminum) TMA/Water precursor at 250 ^{o}C. On top of the Al_2O_3, a semi-transparent top-gate (10nm of Au) is deposited via ebeam evaporation following optical (ebeam) lithography patterning. Next, the source and drain electrodes are exposed through the dielectric layer by RIE etching of Al_2O_3 using BCl_3 by Oxford Plasmalab 100 ICP etcher, on a mask pattern using optical (ebeam) lithography.

Characterization: Given in Supplementary Information, Section 3.

References:

1. Novoselov, K. S. *et al*. A roadmap for graphene. *Nature* **490,** 192-200 (2012).
2. Bonaccorso, F. *et al*. Graphene, related two-dimensional crystals, and hybrid systems for energy conversion and storage. *Science* **347,** 6217 (2015).
3. Tongay, S. *et al*. Rectification at Graphene-Semiconductor Interfaces: Zero-Gap Semiconductor-Based Diodes. *Phys. Rev. X,* **011002** (2012).
4. Yang, H. *et al*. Graphene Barristor, a Triode Device with a Gate-Controlled Schottky Barrier. *Science* **336**, 1140 (2012)
5. Sinha, D. & Lee, J. U. Ideal Graphene/Silicon Schottky Junction Diodes. *Nano Lett*. **14,** 4660 -4664 (2014).
6. Li, X. *et al*. Graphene-On-Silicon Schottky Junction Solar Cells. *Adv. Mater.* **22,** 2743 – 2748 (2010).
7. Miao, X. *et al*. High Efficiency Graphene Solar Cells by Chemical Doping. *Nano lett.***12,** 2745 - 2750 (2012).
8. Zhou, S. Y. *et al*. Substrate-induced bandgap opening in epitaxial graphene. *Nature Mater.* **6**,770–775 (2007).
9. Schedin, F. *et al*. Detection of individual gas molecules adsorbed on graphene. *N. Mater.* **6,** 652-655 (2007).
10. Wang, H., Maiyalagan, T. & Wang, X. Review on Recent Progress in Nitrogen-Doped Graphene: Synthesis, Characterization, and Its Potential Applications. *ACS Catalysis* **2,** 781 - 784(2012).
11. Kim, Y., Yoo, J.M., Jeon, H.R. & Hong, B.H. Efficient n-doping of graphene films by APPE (aminophenyl propargyl ether): a substituent effect. *Phys. Chem. Chem. Phys.* **15,** 18353-18356 (2013).
12. Dong, X. *et al*. Doping Single-Layer Graphene with Aromatic Molecules. *Small* **5,** 1422 - 1426 (2009).
13. Caragiu, M. & Finberg, S. Alkali metal adsorption on graphite: a review. *J. Cond. Mater. Phys.* **17,** R995–R1024 (2005).
14. Uchoa, B., Lin, C. Y. & Castro Neto, A. H. Tailoring graphene with metals on top. *Phys. Rev. Lett.* **77,** 035420 (2008).
15. Sung, S. J. *et al*. Band gap engineering for graphene by using Na+ ions. *Appl. Phys. Lett.* **105,** 081605 (2014).
16. Breitholtz, M., Kihlgren, T., Lindgren, S-Å. & Walldén, L. Condensation of Na metal on graphite studied by photoemission. *Phys. Rev.* B. **67,** 235416 (2003).
17. Johnson, M., Stanberg, M. & Huges, H. Electronic-Structure of Alkali-metal Overlayers On Graphite Surface Science. *Surface Science* **178,** 290-299 (1999).
18. Granath, K., Bodegard, M. & Stolt, L. The effect of NaF on Cu(In, Ga)Se_2 thin film solar cells. *Sol. Eng. Mater. Sol. Cells*. **60,** 279 - 293 (2000).

19. Wei, S., Zhang, S. & Zunger, A. Effects of Na on the electrical and structural properties of $CuInSe_2$. *J. of Appl. Phys.* **85,** 7214 - 7218 (1999).

20. Kronik, L., Cahen, D. & Schock, H.W. Effects of sodium on polycrystalline $Cu(In,Ga)Se_2$ and its solar cell performance. *Adv. Mater*. **10,** 31 - 36 (1998).

21. Niles, D. *et al*. Na impurity chemistry in photovoltaic CIGS thin films: Investigation with x-ray photoelectron spectroscopy. *J. Vac. Sci. Technol. A.* **15,** 3044 - 3049 (1997).

22. Spanu, L., Sorella, S. & Galli, G. Nature and Strength of Interlayer Binding in Graphite. *Phys. Rev. Lett.* **103,** 196401 (2009).

23. Witte, W., , R. & Raman, M. P. Investigations of $Cu(In,Ga)Se_2$ thin films with various copper contents. *Thin Solid Films* **517,** 867 - 869 (2008).

24. Ferrari,A. C. *et al*. Raman Spectrum of Graphene and Graphene Layers. *Phys. Rev. Lett*. **97,** 187401 (2006).

25. Kohn, W. & Lau, K. H. Adatom Dipole Moments on Metals and Their Interactions. *Solid State Commun.* **18**, 553 - 555 (1976).

26. Nadenau, V., Rau, U., Jasenek, A. & Schock, H.W. Electronic properties of $CuGaSe_2$-based heterojunction solar cells. Part I. Transport analysis. *J. Appl. Phys.* **87,** 584 - 593 (2000).

27. Siebentritt, S. & Rau, U. Wide-Gap Chalcopyrites (Springer Series in Materials Science). **86**, (2006)

28. Yu, Y. *et al*. Tuning the Graphene Work Function by Electric Field Effect. *Nano Lett*. **9,** 3430 -3434 (2009).

29. Hinuma, Y., Oba, F., Kumagai, Y. & Tanaka, I. Ionization potentials of (112) and (112) facet surfaces of $SuInSe_2$ and $CuGaSe_2$. *Phys. Rev. B.* **86,** 245433 (2012).

30. Heske, C., Fink, R., Umbach, E., Riedl, W. & Karg, F. Na induced effects on the electronic structure and composition of $Cu(In,Ga)Se_2$ thin film surfaces. *Appl. Phys. Lett*. **68,** 3431 - 3433 (1996).

Figure Legends

Figure 1. Surface-transfer n-doping of graphene from Na. **(a)** Conductance (G) (normalized) vs. gate-voltage (V_G) of graphene (GR)/soda-lime glass (SLG) and GR/borosilicate-glass (BSG) (inset) measured in FET configuration (schematic). **(b)** DFT calculated dispersion curve showing n-doping in graphene interacting with Na. **(c)** Na and Se depth-profiles in CIGS/Mo/SLG and CIGS/Mo/BSG from TOF-SIMS. **(d)** Cross-sectional HR-TEM of GR/CIGS/Mo/SLG. **(e)** Raman spectrograph of GR/CIGS/Mo/SLG showing E_0 peak of $CuIn_{0.7}Ga_{0.3}Se_2$ (177 cm^{-1}), and G peak (1585 cm^{-1}) and 2D peak (2665 cm^{-1}) of graphene. **(f)** EDS maps of GR/CIGS/Mo/SLG

showing Na (yellow, top) and C (purple, bottom). **(g)** Schematic of graphene n-doping mechanism on CIGS.

Figure 2. N-doped graphene-CIGS junction. (a) Four-terminal GR/CIGS/Mo/(SLG/BSG) FET. **(b)** SEM of device in panel **(a)**. Scale-bar is 10μm. (Inset) TEM cross section. Scale-bar is 100nm. **(c)** Left: G (normalized) vs. V_G in the dark. Right: Band structure for multi-layer graphene with Fermi-level for each sample in plot to left. **(d)** Graphene (source) - Mo (drain) current-voltage (I-V) curve with(red)/without(blue) the Al_2O_3 top-dielectric under light(solid)/dark(dotted) for GR/CIGS/Mo/SLG. **(e)** Graphene-Mo I-V at different V_G for GR/CIGS/Mo/SLG. **(f)** Photocurrent with V_G =0V bias under 11.14mW cm^{-2} illumination. **(g)** I-V of the GR/CIGS/Mo/SLG under 1000W/m^2 illumination.

Figure 3. Graphene-CIGS junction properties. (a) Data (green circles) and best-fit model prediction (solid blue line) for J_0 (mA/cm^2) vs. T for GR/CIGS/Mo/SLG, using a Landauer transport model (see Eq.(S10)) giving Φ_b = 0.13eV. (Inset) Same data (blue circles) plotted as $\ln(J_o/T^2)$ vs. 1000/T where J_0 is in mA/cm^2 and T is in K, but using an ideal Schottky diode model, $J_o = A^*T^2\exp\left(\frac{-\Phi_b}{kT}\right)$, for the solid green line with best-fit value Φ_b = 0.11eV. (b) Same data (red circles) used in panel (a), but plotted as a modified Arrhenius-plot ($n * \ln(J_O)$ vs. 1000/T), where n is the ideality factor and J_0 is in mA/cm^2; finding the best-fit of Eq. (S12) (solid red line) to the data gives E_a = 0.96eV. (c), Nyquist plot from C-V giving depletion width (W_d) of 190nm. (d) Schematic band structure of multi-layer-GR/CIGS/Mo/SLG interface. φ_{G0}=Work function of intrinsic graphene, φ_G=Work function of graphene, Φ_b=Schottky barrier height, φ_{CIGS} = Work function of CIGS, IP_{CIGS}=Ionization potential of CIGS, E_G=Band gap of CIGS, V_{bi}=Built-in potential.

Acknowledgments: We thank Marcus Bär, Regan Wilks, and Fernando Camino for helpful discussions. We also thank Jesse Claypoole for SIMS and XPS measurements. This work was partially supported by the U.S. Department of Energy, Sustainable Energy Technologies Department under Contract No. DE-SC0012704, and Brookhaven National Laboratory's Laboratory Directed Research and Development (LDRD) Program. Research carried out in part at the Center for Functional Nanomaterials, Brookhaven National Laboratory, which is supported by the U.S. Department of Energy, Office of Basic Energy Sciences, under Contract No. DE- SC0012704.

Contributions

D.M.N.M.D and M.D.E. designed the experiments, analyzed the results, and prepared the manuscript. D.M.N.M.D. designed, fabricated, and characterized the samples. A.A. performed temperature dependent I-V measurement and data analysis. D.D. performed CIGS deposition.

D.D. and H.E. performed metrological characterization of CIGS. K.K. performed TEM sample preparation and imaging. L.Z. performed EDS measurements and TEM analysis. Y.P. performed TEM measurements and DFT calculations. All authors read and approved the final manuscript.

Competing financial interests

The authors declare no competing financial interests.

Corresponding author

Correspondence to: meisaman@bnl.gov, nanditha.dissanayake@gmail.com

Supplementary Information

Spontaneous and strong multi-layer graphene n-doping on soda-lime glass and its application in graphene-semiconductor junctions

D. M. N. M. Dissanayake, A. Ashraf , D. Dwyer, K. Kisslinger, L. Zhang, Y. Pang, H. Efstathiadis, and M. D. Eisaman

Correspondence to: meisaman@bnl.gov and nanditha.dissanayake@gmail.com

This PDF file includes:

Supplementary Text
Figs. S1 to S19
Table ST1

1) Doping density comparison

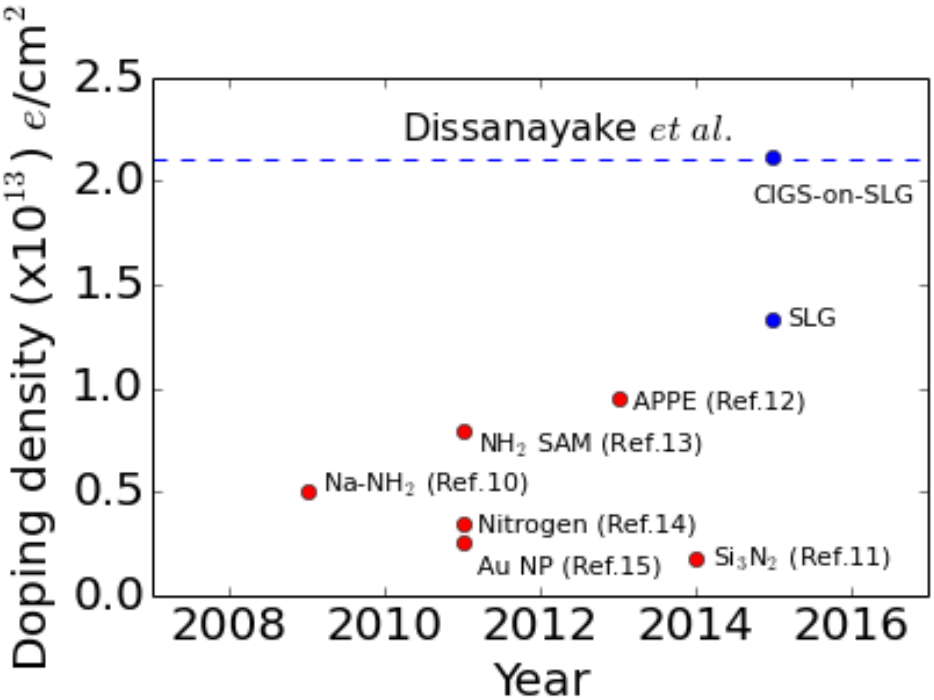

Figure S1. Comparison of n-doping density. Past chemical-doping strengths (red dots) compared to the strength of n-doping achieved in this work (blue dots) via Na surface-transfer doping from soda-lime glass (SLG) and CIGS-on-SLG. APPE = Aminophenyl propargyl ether.

2) CIGS deposition on Mo/SLG

The CIGS films used in these devices were deposited using three-stage thermal co-evaporation from elemental sources of Cu, In, Ga, and Se onto a heated Mo-coated soda-lime glass substrate (SLG). The SLG used was purchased from Guardian (product name: Ecoguard Mo-1, 3.0mm thickness) consisting of nominally ~15% Na_2O (Ref. S1). The glass was coated with a Mo film by the glass manufacturer to a thickness of ~330nm (resistivity 15-22 μΩ-cm). The combined CIGS/Mo film thickness is typically measured to be 2.0μm, with Cu ratio (Cu/(In+Ga)) of 0.94, and Ga ratio (Ga/(Ga+In)) of 0.30 as measured by X-ray Fluorescence (XRF) (e.g. Sample # I1291 shown in Figure S1). XRF is used to measure copper and gallium ratios using a Ceres Technologies System SMX (Model #C06-01915-4002). The system was calibrated for CIGS films using the Standard–adjusted FP (fundamental parameters) method[2,3] CIGS films of different compositions and thicknesses were measured using XRF. The film thickness was then measured using a stylus profilometer, and the film composition was measured using an inductively-coupled plasma (ICP) spectrophotometer with CIGS standard solutions. The

XRF system was calibrated using these values. When these same CIGS layers are

incorporated into standard (Mo/CIGS/CdS/iZnO/AZO) devices, the current-voltage curves yield power conversion efficiencies in the range of 15-18%.

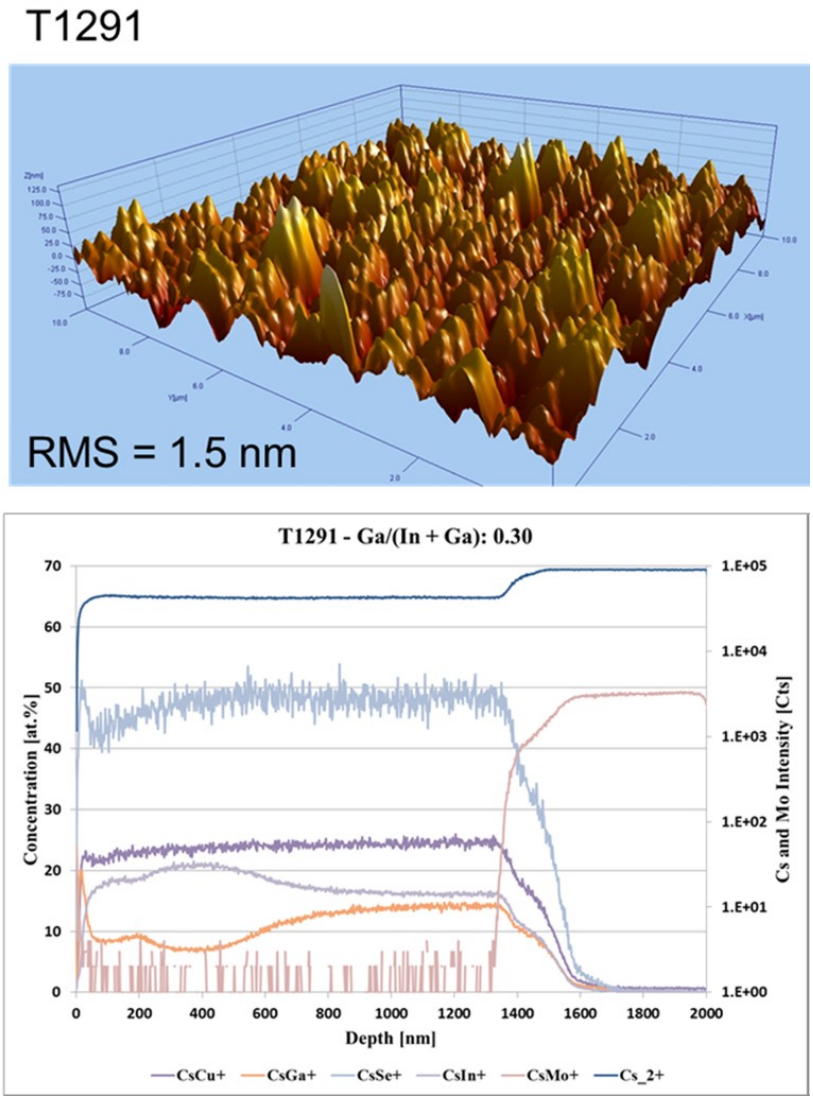

Figure S2. AFM and TOF-SIMS on CIGS/Mo/SLG substrate.

2) Device fabrication

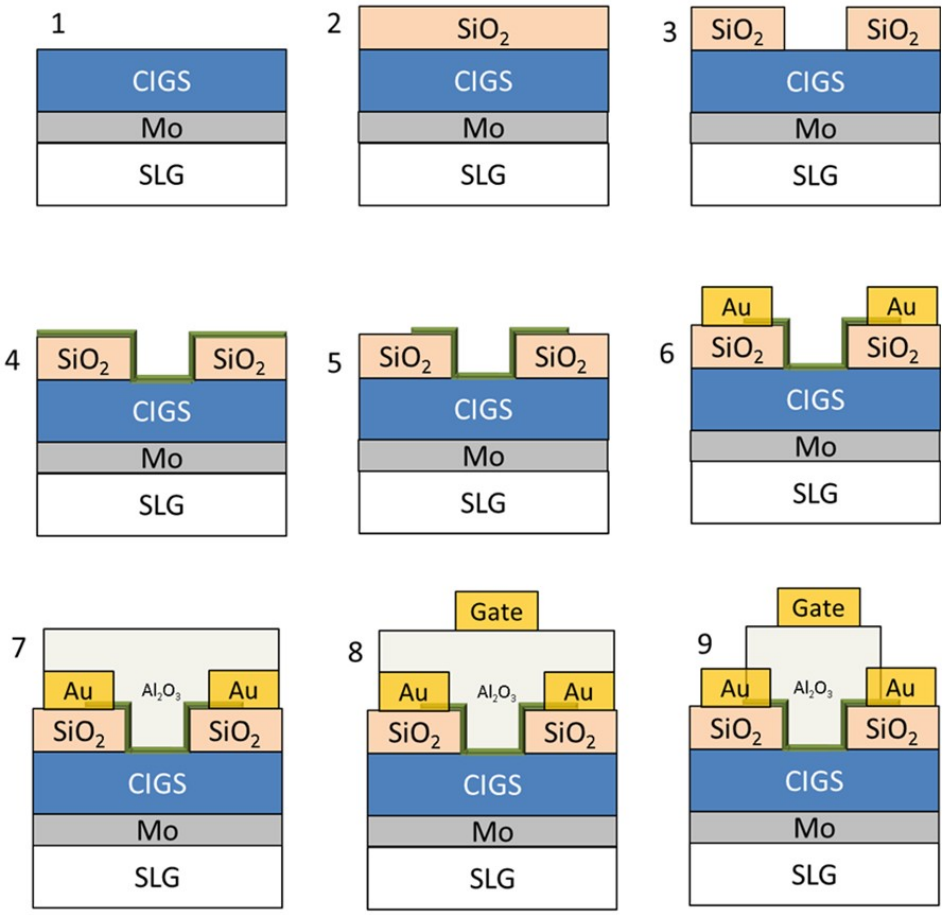

Figure S3. Device fabrication steps for GR/CIGS/Mo/SLG. (1) Clean the CIGS/Mo/SLG via Acetone and IPA. **(2)** Deposit 400 nm of SiO_2 using PECVD. **(3)** Optical/Ebeam lithographically pattern substrates and etch the SiO_2 to expose CIGS devices areas (i.e. 10µm^2, 100µm^2, etc.). **(4)** Wet-transfer CVD graphene (green line) on the opening. **(5)** Optical/Ebeam pattern and etch of the CVD graphene. **(6)** Optical/Ebeam lithographic pattern and deposit Cr (3 nm)/Au (30 nm) contacts on graphene. **(7)** Deposition of 200 nm of Al_2O_3 using ALD. **(8)** Optical/Ebeam lithography of the top-gate contact. **(9)** Optical/EBeam lithography and etch of the Al_2O_3 to expose the Au contacts.

3) Characterization methods

TEM

TEM thin-film samples were made via FIB using a FEI Helios Nanolab 600 Dualbeam (FIB/SEM) system employing a standard in-situ lift-out technique. Initial bulk milling was performed at 30 keV using a liquid metal gallium source. The specimen was subsequently cut free and transferred to a copper grid with a sharpened tungsten Omniprobe needle. Once attached to the TEM grid, the sample was thinned with progressively lower beam voltages down at to an approximate thickness of 50 nm with final milling performed at 2 keV. TEM images were acquired on a JEOL JEM2100F HRTEM operating at an accelerating voltage of 200 keV utilizing a 2K x 2K CCD camera.

EDS

The energy-dispersive X-ray spectroscopy (EDS) chemical maps were acquired on a Hitachi2700C-STEM operated at 200kV.

SIMS

A Physical Electrons 6650 Quadrupole SIMS was used to calculate the concentration of Na with respect to depth in the CIGS and glass samples. A CIGS and Obsidian implanted standard was used to determine the sputter rate and concentration of Na in the samples. The samples were first loaded into the sample exchange chamber and pumped down to 10^{-8} torr before being inserted to the main chamber. Cesium bombardment with a 60 degree angle of incidence, an accelerating voltage of 5 keV, and a beam current of 450 nA was used at 10^{-9} Torr in order to create the ions. The area scanned by the cesium beam had a raster size of 500x500µm and a 10% gate detection area. Charging at the surface was reduced using an electron beam. An electron multiplier detector was used to detect the positive secondary ions.

I-V

Low temperature current-voltage (I-V) measurements were performed using the MMR technologies variable temperature micro-probe system. The temperature is varied from 83-300K in steps of 10K using a micro miniature refrigerator that cools the sample using the Joule-Thompson expansion of high-pressured nitrogen gas (chamber pressure <1mTorr). At each temperature an IV curve is extracted using a Kiethley 2600 source meter.

RAMAN

Raman measurements were made using a WiTec Probe confocal Microscope at 514nm at 100x magnification. The optical power was kept at threshold in order not to locally heat the sample.

4) XPS measurements on SLG SIMS calibration

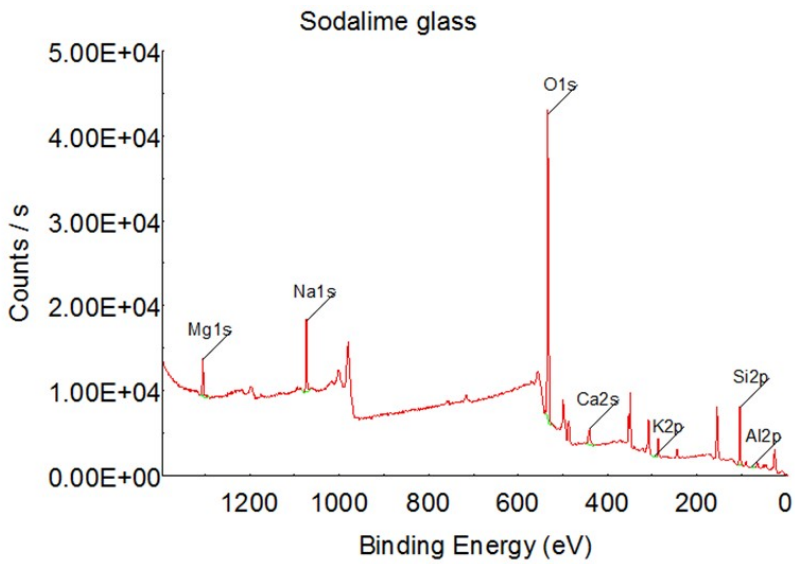

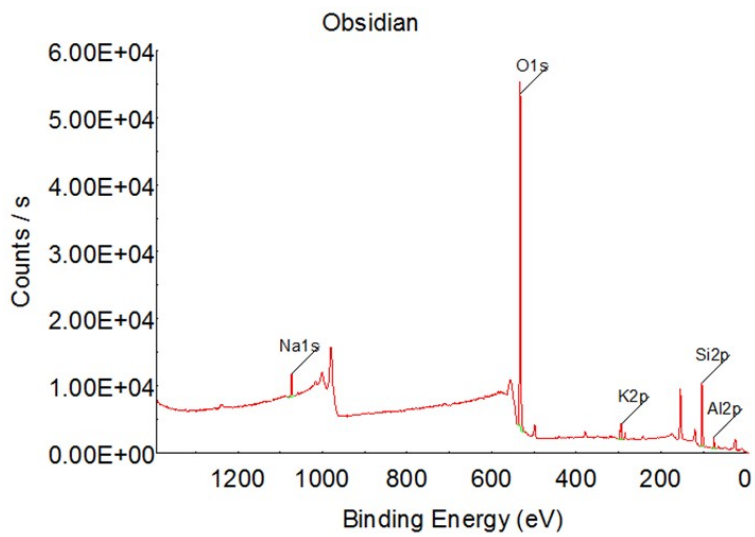

Figure S4. XPS analysis of the top 10 nm of soda-lime glass and calibration sample Obsidian.

Soda-lime glass (after removing ~25nm top layer by Ar+ sputtering)

- Used Obsidian reference to obtain sensitivity factors for all elements except Ca and Mg (XPS was not sensitive enough to detect Ca and Mg).
- Using SiO_2 density the following where measurements were obtained
- 8% wt. of Na_2O (≤2.5%)
- 1.15×10^{21} Na atoms/cm^3 (~5% atomic Na) for SLG

TOF-SIMS measurements

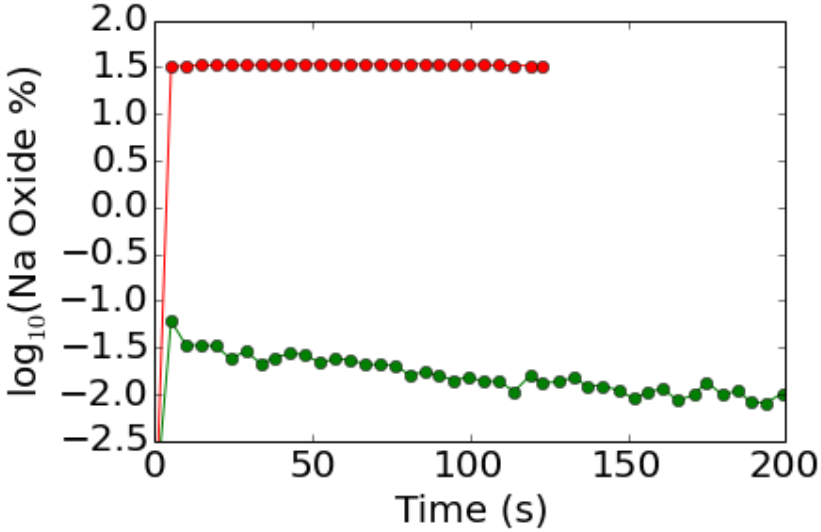

Figure S5. Na depth-profiles in SLG (red) and BSG (green) from (TOF)-SIMS. Data is calibrated using XPS analysis (Fig. 4) giving 1.15×10^{21} and 2.30×10^{20} Na atoms/cm^3 in the SLG and BSG respectively.

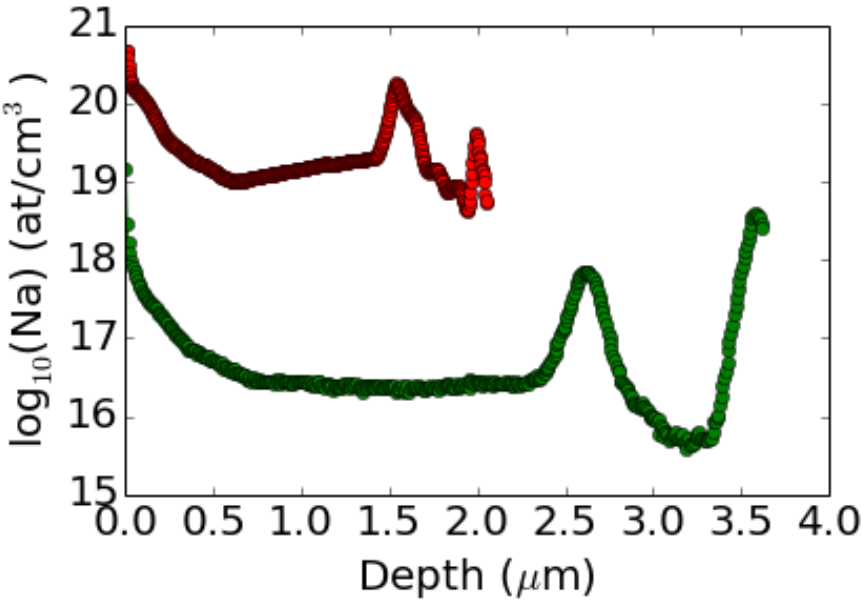

Figure S6. TOF-SIMS measurement on the CIGS/Mo/SLG (Ecoguard Mo-1, 3.0mm thickness and model and Na_2O 8%) (Red) and CIGS/Mo/Borosilicate glass (Green) (Corning 1737, with <1% Na_2O). Na peak at the CIGS-Mo edge at (1.5μm, 2.5μm) in (red, green) curve is from trace Na impurities in the Mo sputter target localized near the Mo-CIGS interface.

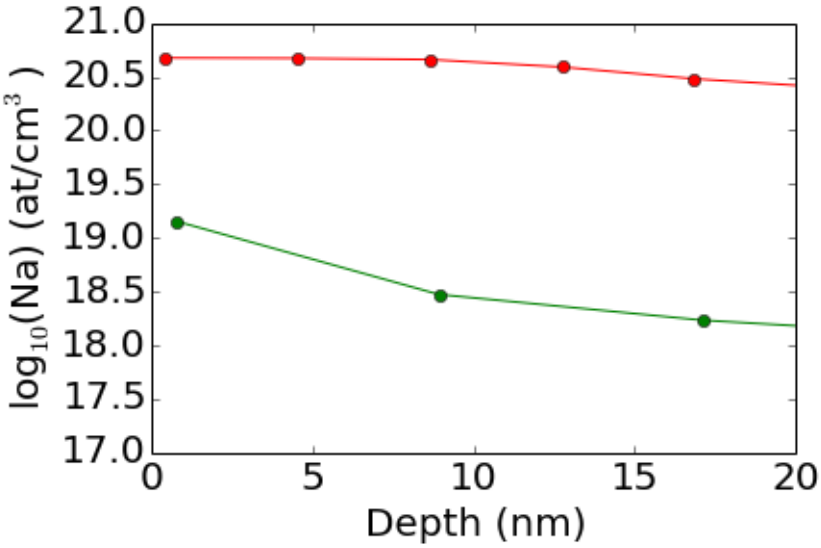

Figure S7. SIMS measurement on the top 20 nm of CIGS/Mo/SLG (Red, 8% Na_2O) (red-curve) and CIGS/Mo/Borosilicate glass (Corning 1737, with <1% Na_2O) (green-curve). SLG surface Na density at 1nm is $4.18 \times 10^{13} cm^{-2}$, BSG surface Na density at 1nm is 6.16×10^{11} cm^{-2}.z

5) Transconductance measurements

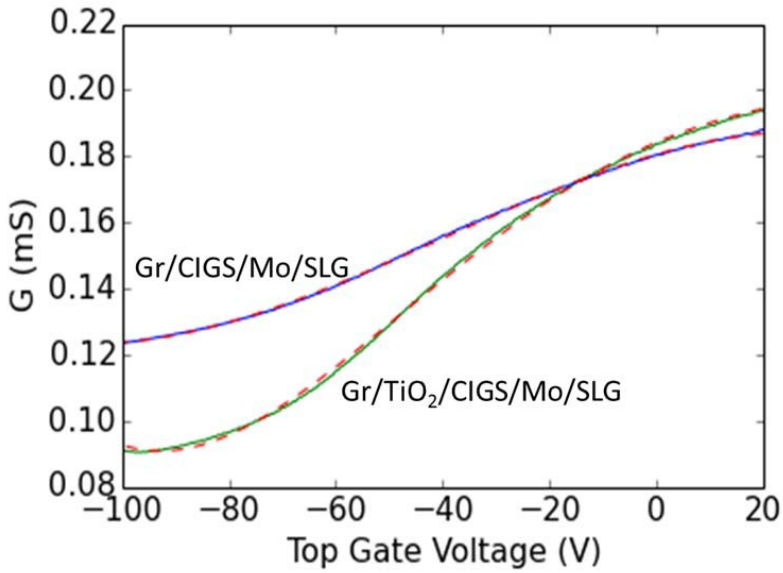

Figure S8. GR/CIGS/Mo/SLG (blue) and GR/TiO_2/CIGS/Mo/SLG (green) transconductance measurements at 10 mV source-drain bias at room-temperature in the dark. Dirac point of GR/CIGS/Mo/SLG is -106V and GR/TiO_2/CIGS/Mo/SLG is -92 V by a polynomial fit to the data. TiO_2 thickness is 4 nm.

The shift in the Fermi Energy (ΔE_F) can be written using Eq. (S1) where v_F is the Fermi velocity (v_F ::: $0^6 m/s$ for graphene), N is the charge density of graphene, and $\hbar$ is Planck's constant[4].

$$\Delta E_F = \hbar v_F \sqrt{rrN} \tag{S1}$$

In Eq. (S1) the charge density N is calculated considering the capacitance of the top dielectric (C_{TOP}) and the applied potential (V) considering a parallel-plate capacitor with ($N = \epsilon_o \epsilon AV/d$) where ϵ_o, ϵ, A, d and V are vacuum permittivity ($\epsilon_o = 8.854 \times 10^{-12}$ F/m), relative dielectric constant ($\epsilon = 9.1$), cross-sectional area ($A = 10^4$ μm^2), and thickness of the dielectric (d = 252nm from TEM measurements).

At the asymptotic top-gate potential at the charge neutrality point (-106 V), N and ΔE_F are calculated as 2.11×10^{13} e/cm^{-2} and 536meV, respectively for the GR/CIGS/Mo/SLG substrate. From this calculation, the graphene Fermi level at the charge neutrality point of -106 V is shifted up by ΔE_F = +536meV, with respect to un-doped graphene.

6) Helmholtz equation to calculate the graphene work-function shift on GR/CIGS/SLG (BSG)

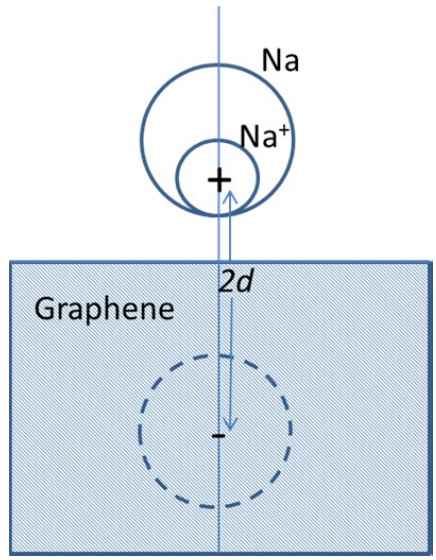

Figure S9. Change of the potential on graphene due to the dipole moment from Na^+ and image-charge.

The change of the potential on graphene due to the dipole moment from Na^+ and image-charge is given by:

$$\Delta\Phi = \frac{2rreN_a\mu(8)}{EE_0},$$

where *Llct* is the change in the Graphene work function, μ is the dipole-moment of the Na^+ and the image force on graphene, E is the relative dielectric constant, $E_o$is the vacuum permittivity, e is electron charge, N_a is the density of the ions per unit area on CIGS, and e is the fractional coverage of the ions on graphene.

$$\mu(e) = 2dqN_a,$$

where d is the distance between graphene and the Na ion, and q is the charge of an electron. Taking d = 0.1 nm (i.e. the Na^+ radius is 98 pm and elemental Na radius 186 pm), q = 1.6 X 10^{-19} C, N_a = 4.18x10^{13} cm^2 (CIGS/SLG) and 6.16x$10^{11}$$cm^2$ (CIGS/BS), $E = 13.6$ and $E_o = 8.854 * 10^{-12}$ F/m, and e is taken as 1.0 (complete coverage). e varies from 0.25-1.0 in previous studies[5]. The change in the graphene work function is calculated to be:

- *Llct* for CIGS/SLG = 0.69 eV
- *Llct* for CIGS/BSG = 0.01 eV.

7) GR/CIGS/Mo/SLG photovoltaic device measurements

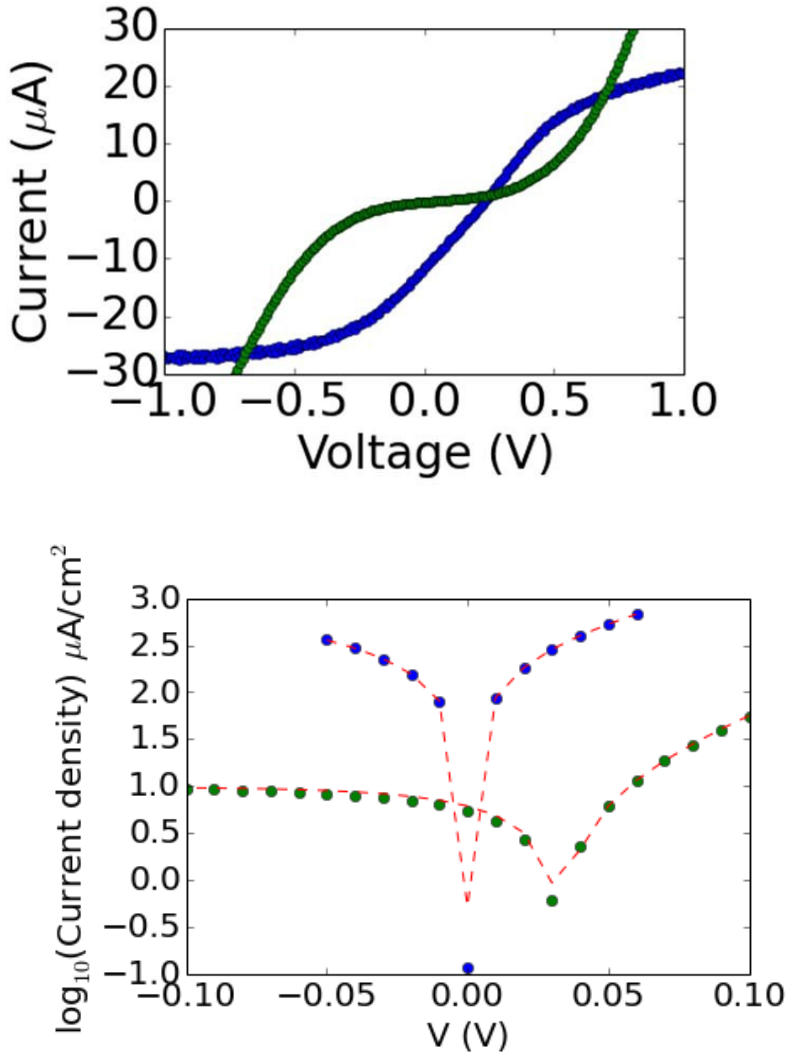

Figure S10. Linear photovoltaic current-voltage (I-V) behavior of the GR/CIGS/Mo/SLG (top). Blue curve is before Al_2O_3 and green curve is after Al_2O_3 under 11.14 mW/cm^2 illumination. After Al_20_3, $J_0 = 3.59x10^{-10}$ (A/cm^2) and ideality-factor A=1.29. Before Al_20_3: J_0= $1.23x10^{-6}$ (A/cm^{-2}) and A=91.53 fitting to the low-bias region (bottom).

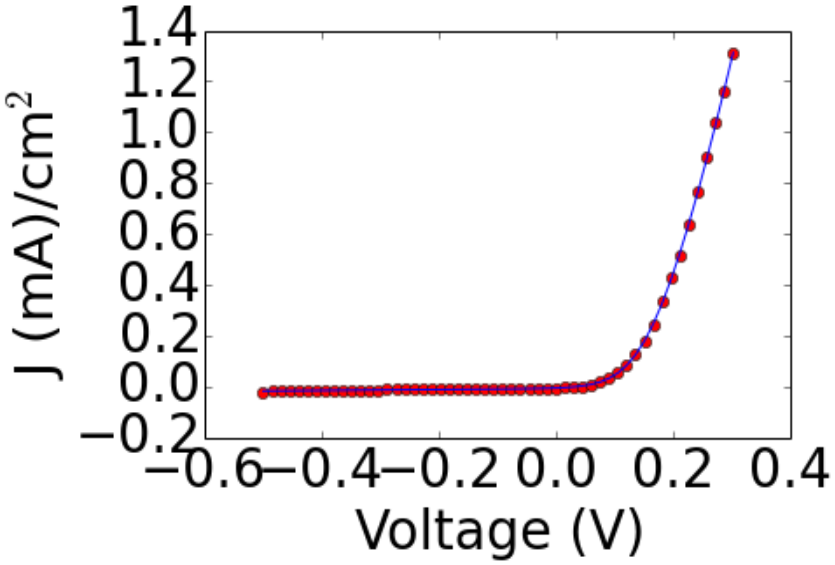

Figure S11. Dark I-V of GR/CIGS/Mo/SLG device with an ideality factor of A=1.21.

8) V_G dependent I-V measurement in GR/CIGS/Mo/SLG

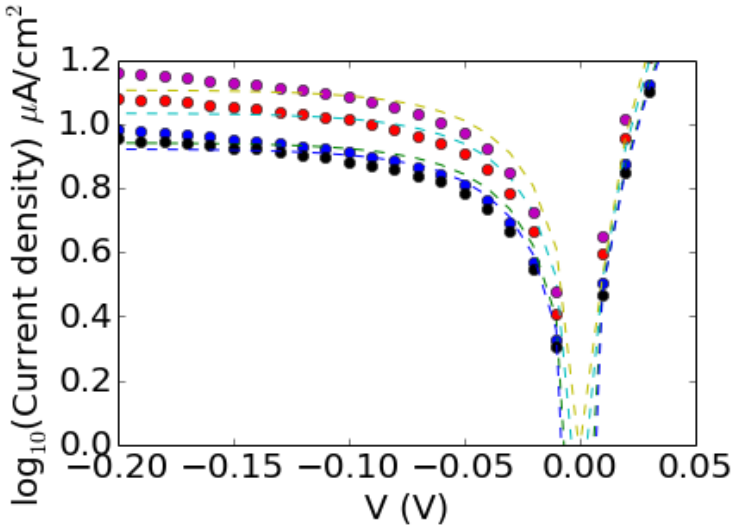

Figure S12. I-V behavior in the dark with different top-gate potentials shown in Table T1.

V_G (V)	J_0 (A/cm^2)	n	Data point color
50	8.2 x 10^{-10},	1.22	black
0	8.56x10^{-10},	1.21	blue
-50	1.02 x10^{-9},	1.22	red
-100	1.17 x10^{-9}	1.23	purple

Table ST1. Fitting parameters at different V_G. *n* is the ideality factor, V_G is gate-voltage, and J_0 is the reverse saturation current density.

J_0 vs. V_G relationship at constant T

Graphene/CIGS can be modeled as an n-type metal and p-type semiconductor Schottky diode in which the I-V is behaving as given in Eq. (S2) where *T* is temperature, *k* is the Boltzmann coefficient, *q* is the charge of an electron, *V* is the applied bias, *A* is the contact area and *n* is the ideality factor. J_0 is the reverse saturation current density, which is given in Eq. (S3), where Φ_b is the Schottky barrier height, and A^* is the Richardson coefficient.

$$= \quad {}_{o}\,\text{\textcircled{?}}\,exp\left(\frac{qV}{nkT}\right) - 1] \tag{S2}$$

$$_{o} = \quad {}^{*}\ {}^{2}exp\left(\frac{-<p_b}{kT}\right) \tag{S3}$$

Φ_b is given by Eq. (S4), where $<p_G$ is the Fermi level of graphene and *x* is the ionization potential of CIGS. As given in Eq. (S5), the Fermi level of graphene has an intrinsic component given by $<p_{Go}$ and a top-gate tunable electrostatic shift of the work function (Ll_F) which is given by Eq. (S6), where *n* is the ideality factor, $\hbar$ is the modified Planck's constant, V_F is the Fermi velocity in graphene, and *N* is the charge density.

$$ct_b = x - <p_G \tag{S4}$$

$$<p_G = <p_{Go} - LlE_F \tag{S5}$$

The charge density *N* is a function of V_G as given by Eq. (S7), where ϵ, ϵ_o, A, V_G, *d*, and ΔE_F are the relative dielectric constant, vacuum permittivity, area, gate-bias, thickness of the top dielectric, and the Fermi energy shift due to n-doping, respectively.

$$LlE_F = eLlV_F = \hbar v_F\sqrt{rrN} \tag{S6}$$

$$N = \frac{EE\ A(V\ +LlV\ )}{d}, \tag{S7}$$

where LlV_F represents the offset voltage in the doped graphene due to the Fermi energy shift, *e* is the electron charge (1.6 x 10^{-19} C), ñ is Planck's constant (4.14 x 10^{-15} eV s), and v_F is the Fermi velocity (v_F ::: $0^6 m/s$ for graphene). Combining Eqs. (S4-S7) with Eq. (S3) gives an equation between V_G and J_0 given in Eq. (S8). Plotting, $\ln(J_o)$ vs. $(|V_G + \Delta V_F|)^{1/2}$ should be a line with an intercept equal to $\ln(A^*T^2) - (x-<p_{Go})/kT$, as shown in Eq. (S9). Therefore, we are able to obtain the value of the ct_{bo}, which is the Schottky barrier of the n-doped device at zero-gate bias, independent of the conventional temperature dependent I-V characteristics.

$$_{o} = \quad {}^{*}\ {}^{2}e \quad \frac{-(x-<p_{GO})-\hbar v_F \frac{\cancel{\pi rEE_OA(V_G+.1V_F)}}{d}}{kT} \tag{S8}$$

$$ln(\ _o) = ln(\ ^*\ ^2) + \quad - ct_{bo} - \hbar v_F \quad \frac{\overline{rEE_0A(V_G+LlV_F)}}{d} \boldsymbol{j}k \qquad \text{(S9)}$$

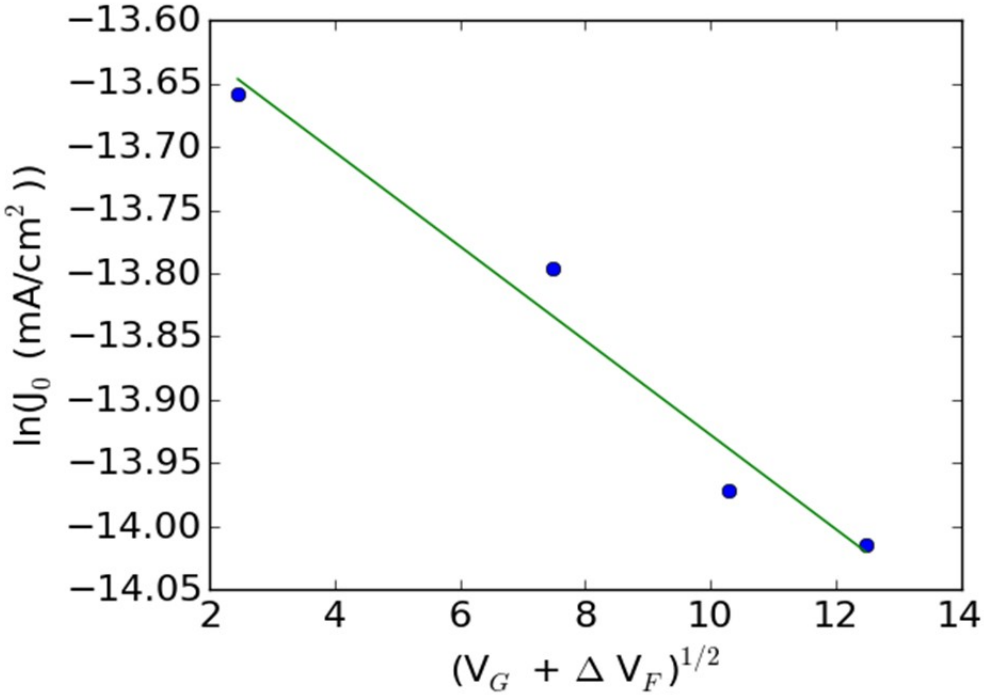

Figure S13. $\ln(J_0)$ vs. $(|V_G + LlV_F|)^{1/2}$.

Taking the Richardson constant (A^*) as $A^*=1.18\text{x}10^{-6}$ $mAcm^{-2}K^{-2}$ (from the temperature dependent analysis in Fig. S15), the intercept in Fig. S13 at $(V_G + \Delta V_F)=0$ is -13.56:

$$-13.56= -ct_{bo}/k \ + \ln(300 \text{ x } 300 \text{ x } 1.18 \text{ x } 10^{-6}) = -ct_{bo}/k \ + \ln(0.106)$$

$$ct_{bo}/k \ = 13.56 - 2.24 = 11.31$$

$$ct_{bo}= 11.31 \text{ x } 26 \text{ meV} = 0.29 \text{ eV}$$

9) Recombination analysis on GR/CIGS/Mo/SLG

For an ideal Schottky barrier, $_o = \ ^* \ ^2 exp\left(\frac{-<P_b}{kT}\right)$ where ct_b is the Schottky barrier height. By fitting $ln\left(\frac{I_0}{T^2}\right)$ vs. 1000/T, we obtain Schottky barrier height of ϕ_b = 0.11eV and A* = 1.18x10^{-6} mAcm^{-2}K^{-2}. This is assuming a fixed Richardson constant A*.

For finite density of states, A* becomes temperature dependent and the Landauer transport model is used as given in Eq. (S10) below[6]:

$$_o = \frac{qD_o}{T}(k_B\ )^2\left(\frac{ct_B}{k_B} + 1)\right]e^{-ct_B/k_B}\ , \qquad \text{(S10)}$$

where $D_O = [2/(rr(\tilde{N}\ v_F)^2]$ with Ñ Planck's constant and v_F the Fermi velocity (v_F ::: $10^6 m/s$ for graphene) represents the prefactor that gives the graphene density of states when multiplied by the energy, and T is the time scale for carrier injection from the contact. In order to fit this equation to the data shown in the main panel of Fig. 3a, we find the best-fit values for two parameters: $c \equiv \frac{qD_O}{T}$ and ct_B. The blue solid best-fit line shown in the main panel to Fig. 3a is Eq. (S10) with best-fit parameter values of $c \equiv \frac{qD_O}{T}$ = 58.15 and $ct_B = 0.13\ eV$. We observe that the diode quality factor is temperature dependent which means that there is a strong contribution of tunneling in the recombination mechanism. High ideality factors at low temperatures suggest a transition from tunneling dominated interface recombination at low temperatures to standard Shockley-Read-Hall (SRH) behavior at room temperature.

The same J_0 data can be used in a different model where the diode quality factor, n, is taken into account. In this model the reverse saturation current, J_0 can be written as a function of temperature T, activation energy, E_a, the diode quality factor, n, and J_{00}, which is a weakly temperature-dependent prefactor.

$$= \ _O\, exp\left(\frac{qV}{nkT}\right) = \ _{OO}\, exp\left(\frac{-E_a}{nkT}\right) exp\left(\frac{qV}{nkT}\right), \qquad \text{(S11)}$$

Compared to the typical definition of activation energy, where the exponential term containing E_a does not include the ideality factor n in the denominator, Eq. (S11) includes n in the denominator of both exponential terms to account for the temperature dependence of n. In the case of tunneling, where the ideality factor n becomes temperature dependent, we can rewrite Eq. (S11) to obtain

$$n\ ln(\ _0) = \left(\frac{-E_a}{kT}\right) + n\ ln(\ _{00})\ . \qquad \text{(S12)}$$

Assuming that J_{00} is temperature independent, we can extract the activation energy E_a using a modified Arrhenius plot (Ref. S16), $n\ ln(J_0)$ vs. $1/T$ (in contrast to a standard

Arrhenius plot - $ln(J_0)$ vs. $1/T$ – that one would use when the denominator of the exponential term in Eq. (S11) containing E_a does not include the ideality factor n). In an

intrinsic semiconductor, the activation energy is equal to half the bandgap, and for a p-doped semiconductor it should be close to the bandgap energy since the Fermi energy is close to the valence band. We extract an activation energy E_a = 0.96 eV which is lower than the CIGS bandgap of 1.15 eV, suggesting a contribution of tunneling enhanced interfacial recombination (Ref. S16). We note that in our case, and in previous studies[17,18], when extracting E_a for Schottky barrier devices, the difference between E_a and ct_B is largely determined by the value of n and its temperature dependence.

Hole blocking layer between n-graphene and CIGS

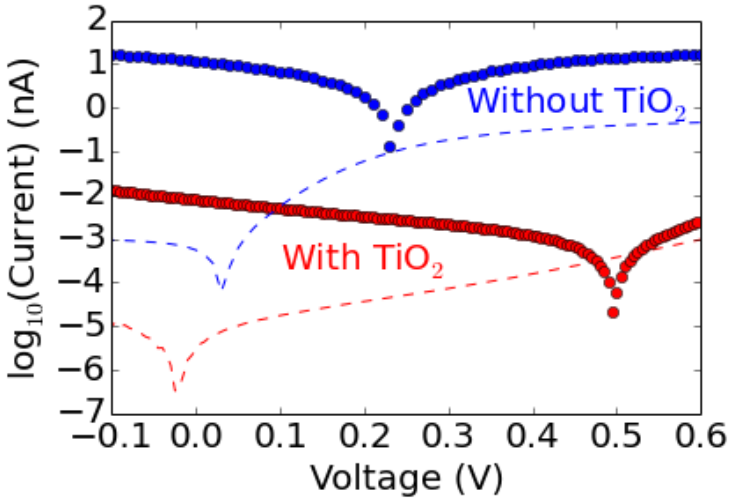

Figure S14. Graphene/CIGS/Mo/SLG (blue) and Graphene/TiO_2/CIGS/Mo/SLG (red) I-V measurements in the dark (dashed) and 11.14 mW white-light (solid). The open circuit voltage without TiO_2 is V_{OC} = 0.23 V, and with a 4nm TiO_2 hole blocking layer V_{OC} = 0.49 V.

10) Density functional theory (DFT) calculations

DFT calculation of a free standing graphene monolayer

The graphene monolayer crystal structure is described by the primitive translation vectors:

$$\underline{a}_1 = a\left(\frac{\sqrt{3}}{2}, \frac{1}{2}\right)$$

$$\overline{a}_2 = a\left(\frac{\sqrt{3}}{2}, \frac{1}{2}\right)$$

$$\overline{a}_3 = a(0,0,6)$$

where a = 2.46Å is the lattice constant. $\overline{a_3}$ is the lattice vector in the z direction, which adds a 6Å vacuum gap between graphene layers. Since we use periodic boundary condition in three directions, the vacuum guarantees that the graphene monolayer is isolated from adjacent layers. The atomic positions are:

$$\overline{\ }_1(C) = (0,0)$$

$$\underline{\ }_2(C) = a\left(\frac{1}{\sqrt{3}}, 0\right)$$

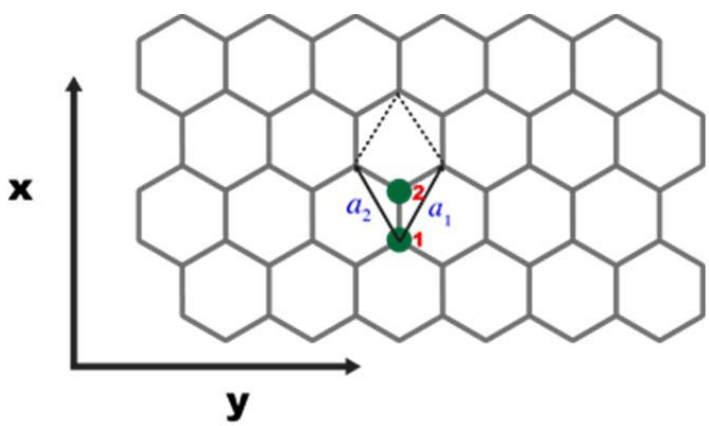

Figure S15. The honeycomb structure of the graphene monolayer. a_1 and a_2 are the two lattice vectors in x,y plane. The primitive unit cell is shown by the lattice vectors and the dotted line and 1 and 2 denote the two carbon atoms per unit cell.

Density functional theory calculation of free-standing graphene with Na

The graphene-monolayer-with -sodium crystal structure is described by the primitive translation vector as shown in:

$$\vec{a}_1 = a\left(\frac{\sqrt{3}}{2}, \frac{1}{2}, 0\right)$$

$$\vec{a}_2 = a\left(\frac{\sqrt{3}}{2}, \frac{1}{2}, 0\right)$$

$$\vec{a}_3 = a(0,0,12)$$

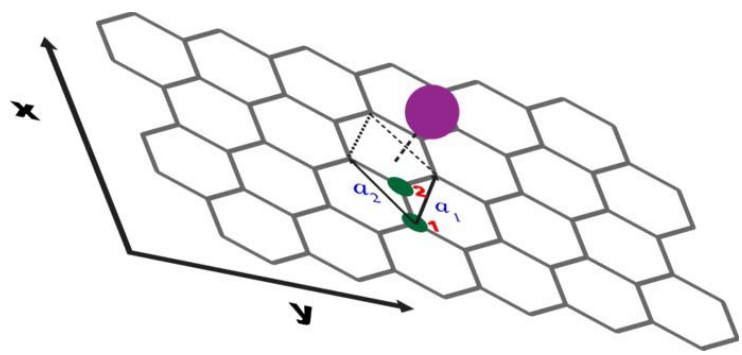

Figure S16. The honeycomb structure of the graphene monolayer with sodium (purple). a_1 and a_2 are the two lattice vectors in x,y plane. The primitive unit cell is shown by the lattice vectors and the dotted line and 1 and 2 denote the two carbon atoms per unit cell; the purple atom is the sodium atom in the primitive unit cell.

Since we introduce the sodium atom into the graphene monolayer crystal structure, we add a thicker vacuum layer (12Å) to isolate the graphene-monolayer-with-sodium system. The atomic positions are:

$$\vec{r}_1(C) = (0,0,0)$$

$$\vec{r}_2(C) = a\left(\frac{1}{\sqrt{3}}, 0, 0\right)$$

$$\vec{r}_3(Na) = a\left(\frac{1}{\sqrt{3}}, 0, 1\right)$$

All the calculations are performed by DFT, which is implemented in GPAW based on the projector-augmented wave (PAW) method and the atomic simulation environment (ASE) (Ref. S7-S9). We use the default Finite Difference mode, which means that the wave

function will be expanded on a real space grid, and the grid spacing is 0.18Å. The Perdew-Burke-Ernzerhof (PBE), which is a generalized gradient approximation (GGA)

type, is adopted. The Brillouin-zone is sampled using Γ-centered 5 × 5 × 1 Monkhorst-Pack k-points. The electrons will be distributed into the available energy levels according to the Fermi Dirac Distribution, and the width kB T = 0.05 eV. The convergence criterion is 1e-12 for the Poisson solver.

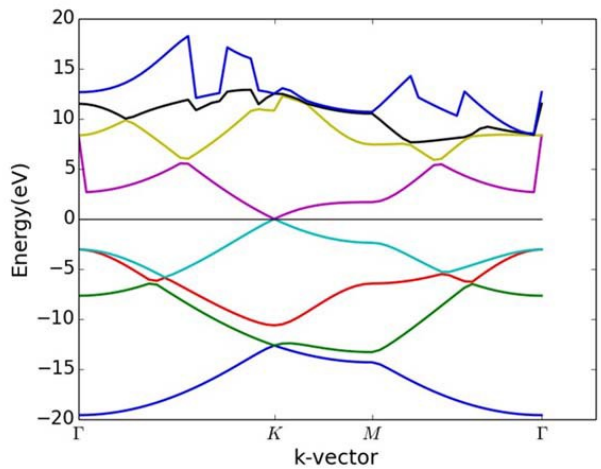

Figure S17. DFT calculation of the band-structure of the graphene monolayer. It clearly shows the linear behavior of the bands near the vicinity of K at the Fermi energy. The conduction and valence bands cross at the Dirac point indicating no intrinsic doping of the structure.

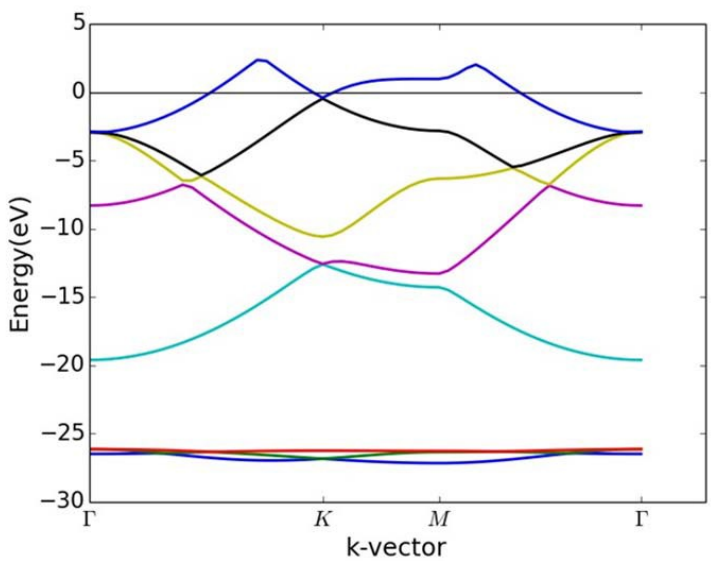

Figure S18. DFT calculation of the band- structure of graphene monolayer interacting with the Na (density: 1 Na atom per primitive unit cell). The result shows a 474meV shift in the Fermi level from the Dirac point at K, which indicates n-doping of graphene from Na.

11) C-V measurements

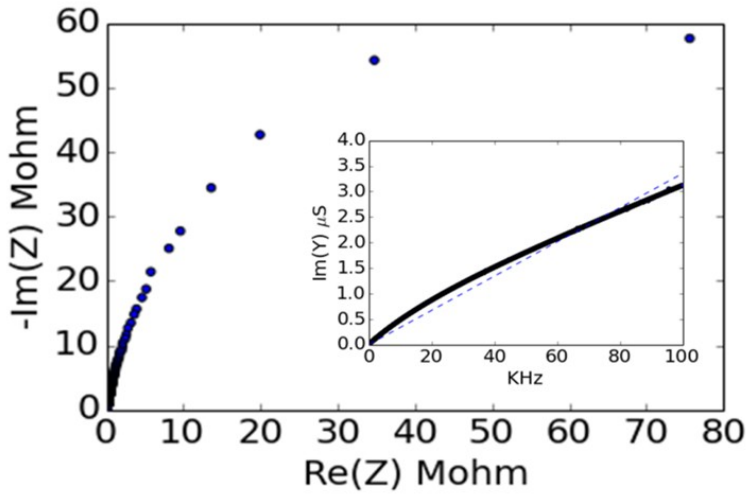

Figure S19. C-V measurement on GR/CIGS/Mo/SLG at 50 mV_{rms} a.c. voltage at 0 V d.c. bias in the frequency range 100 Hz – 100 KHz in dark.

Considering the junction as an RC-equivalent circuit, the junction capacitance *(C_p)* is calculated as 53.32 nF/cm^2 by plotting $Im\left(\frac{1}{Z}\right)$ vs. *f* (inset) using Eq. (S13). Considering uniform charge density in the space-charge region, the space-charge width (W_d) is calculated to be 190.94 nm.

$$Im\left(\frac{1}{Z}\right) = 2rr\ C \qquad \text{(S13)}$$

References

[S1] Al-Thani, H. & Williamson, D. The Effect of Mo Back Contact on Na Out-Diffusion and Device Performance of Mo/Cu, *NREL/CP-520-32254*, (2002).

[S2] Dwyer, D., Schujman, S., Novak, J., Metacarpa, D. and Haldar, P. Selenium flux effects on Cu(In,Ga)Se2 growth rate, and control by in-line X-ray fluorescence, *Proc. of the 39rd IEEE Photovoltaic Specialists Conference* 1957-1960 (2013).

[S3] Gabor, A. *et al*. Band-gap engineering in $Cu(In,Ga)Se_2$ thin films grown from $(In,Ga)_2Se_3$ precursors, *Solar Energy Materials and Solar Cells*. **41/42** 247-260 (1996). [S4] Das, A. *et al*. Monitoring dopants by Raman scattering in an electrochemically top- gated graphene transistor. *Nature. Nanotec.* **3**, (4) 210–215 (2008).

[S5] Caragiu, M. & Finberg, S. Alkali metal adsorption on graphite: a review. *J. of Physics-condensed matter*. **17**, R995–R1024 (2005).

[S6] Sinha, D. & Lee, J. U. Ideal Graphene/Silicon Schottky Junction Diodes. *Nano Lett*. **14**, 4660–4664 (2014).

[S7] Mortensen, J., Hansen, L. & Wedel, K. Real-space grid implementation of the projector augmented wave method. *Phys. Rev. B*. **71**, 035109, (2005).

[S8] Enkovaara, J. *et al*. Electronic structure calculations with gpaw: a real- space implementation of the projector augmented-wave method. *J. of Phys.: Condensed Matter*. **22**, 253202 (2010).

[S9] Bahn, S. & Jacobsen, K. An object-oriented scripting inter- face to a legacy electronic structure code. *Computing in Science & Engineering*. **4**, 56–66 (2002).

[S10] Dong, X. *et al*. Doping Single-Layer Graphene with Aromatic Molecules. *Small* **5,** 1422 - 1426 (2009).

[S11] Wang, Z. *et al*. Air-stable *n*-type doping of graphene from overlying Si_3N_4 film. *Appl. Surf. Sci.* **307,** 712-715 (2014).

[S12] Kim, Y., Yoo, J.M., Jeon, H.R. & Hong, B.H. Efficient n-doping of graphene films by APPE (aminophenyl propargyl ether): a substituent effect. *Phys. Chem. Chem. Phys.* **15,** 18353-18356 (2013).

[S13] Park, J. *et al*. Work-Function Engineering of Graphene Electrodes by Self-Assembled Monolayers for High-Performance Organic Field-Effect Transistors. *J. Phys. Chem. Lett.* **2,** 841–845 (2011).

[S14] Zhang, C. *et al*. Synthesis of Nitrogen-Doped Graphene Using Embedded Carbon and Nitrogen Sources. *Adv. Mater.* **23,** 1020-1024 (2011).

[S15] Huh, S. *et al*. Selective n-Type Doping of Graphene by Photo-patterned Gold Nanoparticles. *ACS Nano* **5,** 3639–3644 (2011).

[S16] Nadenau, V., Rau, U., Jasenek, A. & Schock, H.W. Electronic properties of CuGaSe2-based heterojunction solar cells. Part I. Transport analysis. *J. Appl. Phys.* **87**, 584 - 593 (2000).

[S17] Asghar, M., Mahmood, K., Faisal, M., and Hasan, M. A. Electrical characterization of Au/ZnO/Si Schottky contact. *J. Phys.: Conf. Ser.* **439,** 012030 (2013).

[S18] Wu, C. S. *et al.* Novel GaAs/AlGaAs Multiquantum-Well Schottky-Junction Device and its Photovoltaic LWIR Detection. *IEEE Transactions on Electron Devices* **39**, 234-241 (1992).

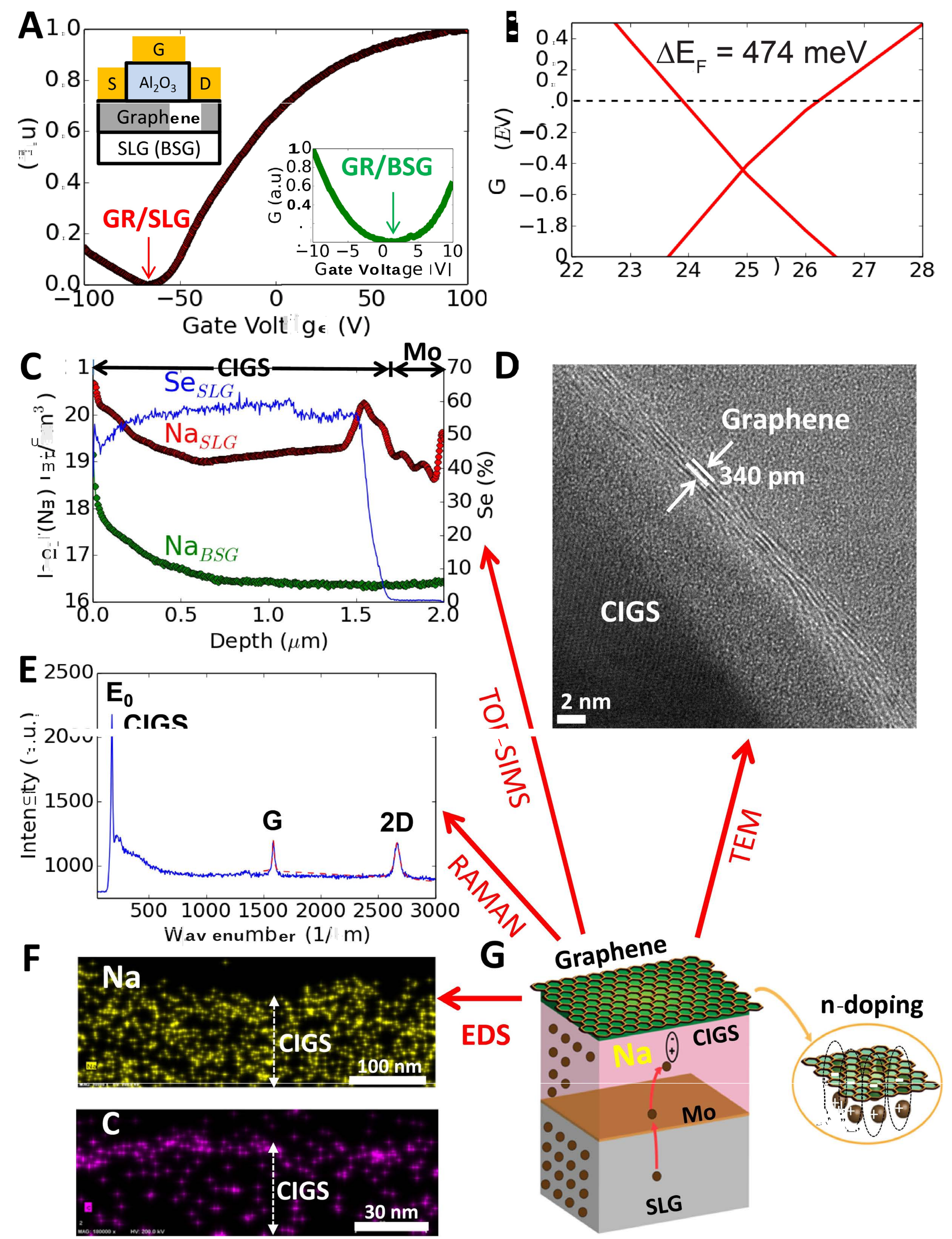
A
G
S
Al_2O_3
D
Graphene
SLG (BSG)
GR/SLG
GR/BSG
G (a.u)
Gate Voltage |V|
Gate Voltage (V)
B
ΔE_F = 474 meV
G (EV)
C
CIGS
Mo
Se_{SLG}
Na_{SLG}
Na_{BSG}
Se (%)
Depth (μm)
D
Graphene
340 pm
CIGS
2 nm
E
E_0
CIGS
G
2D
Intensity (a.u.)
Wavenumber (1/cm)
F
Na
CIGS
100 nm
C
CIGS
30 nm
TOF-SIMS
RAMAN
TEM
EDS
G
Graphene
CIGS
Na
Mo
SLG
n-doping

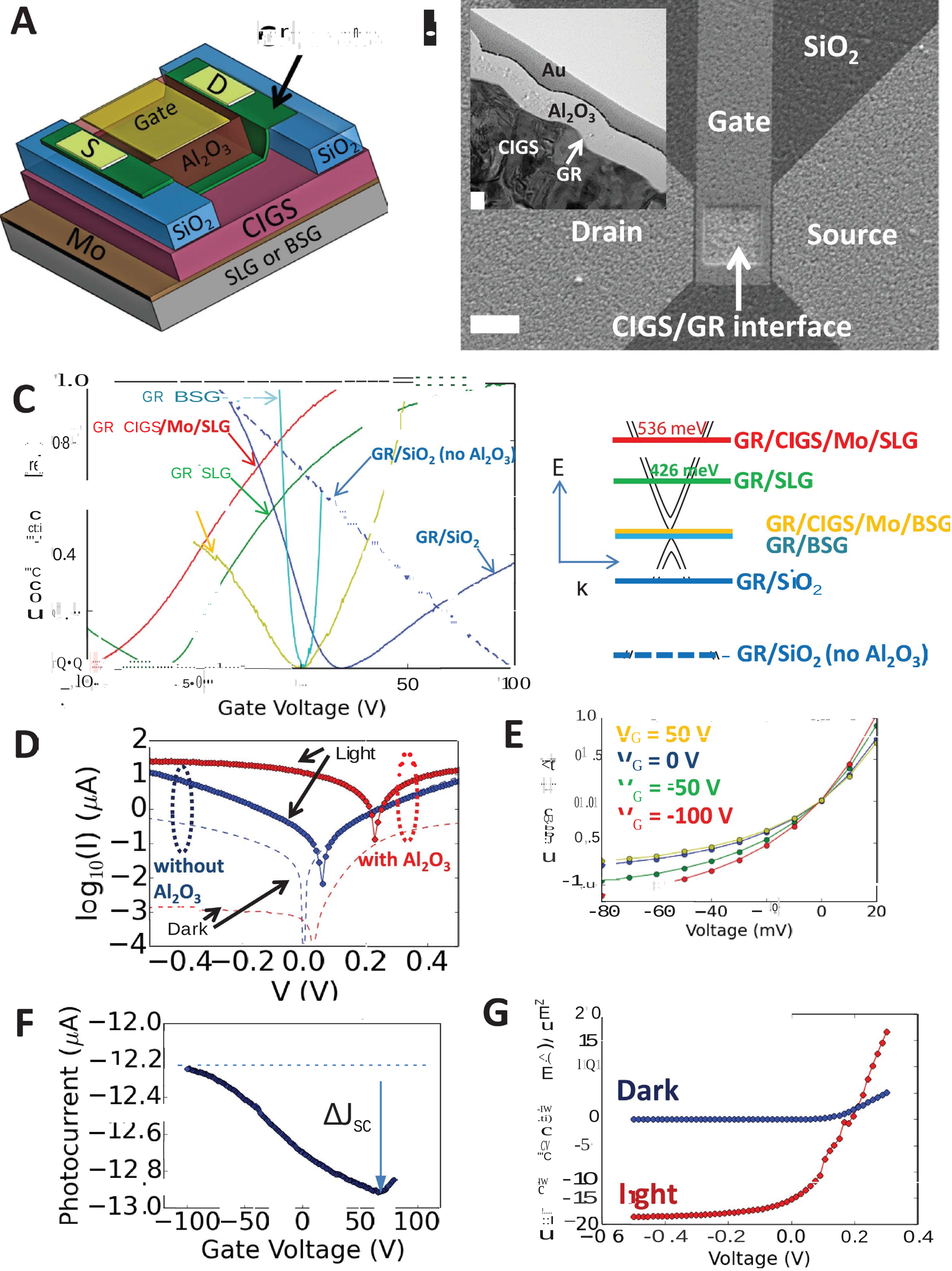
A
D
S
Gate
Al_2O_3
SiO_2
SiO_2
CIGS
Mo
SLG or BSG
B
Au
Al_2O_3
CIGS
GR
SiO_2
Gate
Drain
Source
CIGS/GR interface
C
GR BSG
GR CIGS/Mo/SLG
GR SLG
GR/SiO_2 (no Al_2O_3)
GR/SiO_2
Gate Voltage (V)
536 meV
426 meV
E
k
GR/CIGS/Mo/SLG
GR/SLG
GR/CIGS/Mo/BSG
GR/BSG
GR/SiO_2
GR/SiO_2 (no Al_2O_3)
D
Light
without Al_2O_3
with Al_2O_3
Dark
$\log_{10}(I)$ (μA)
V (V)
E
V_G = 50 V
V_G = 0 V
V_G = -50 V
V_G = -100 V
Voltage (mV)
F
Photocurrent (μA)
ΔJ_{SC}
Gate Voltage (V)
G
Dark
light
Voltage (V)

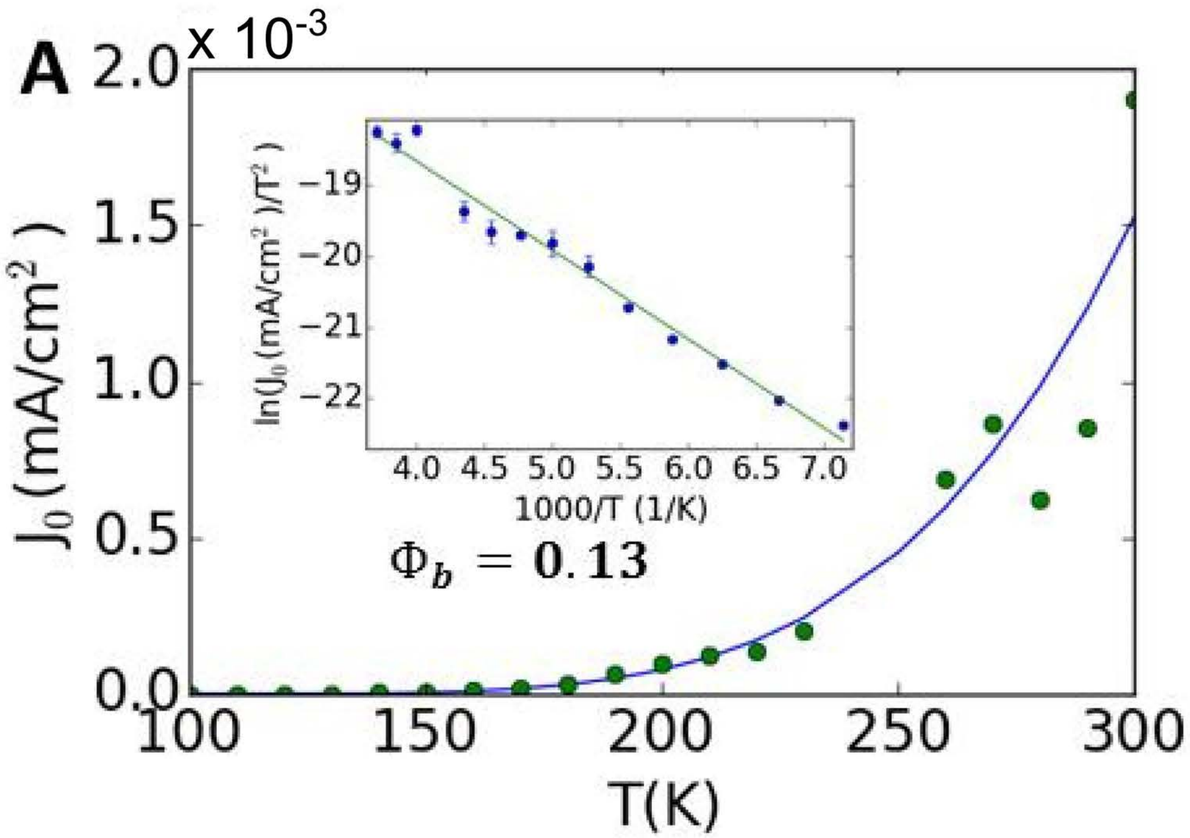
A
x 10-3
2.0
1.5
1.0
0.5
0.0
J0 (mA/cm2)
100
150
200
250
300
T(K)
ln(J0 (mA/cm2)/T2)
−19
−20
−21
−22
4.0 4.5 5.0 5.5 6.0 6.5 7.0
1000/T (1/K)
Φb = 0.13

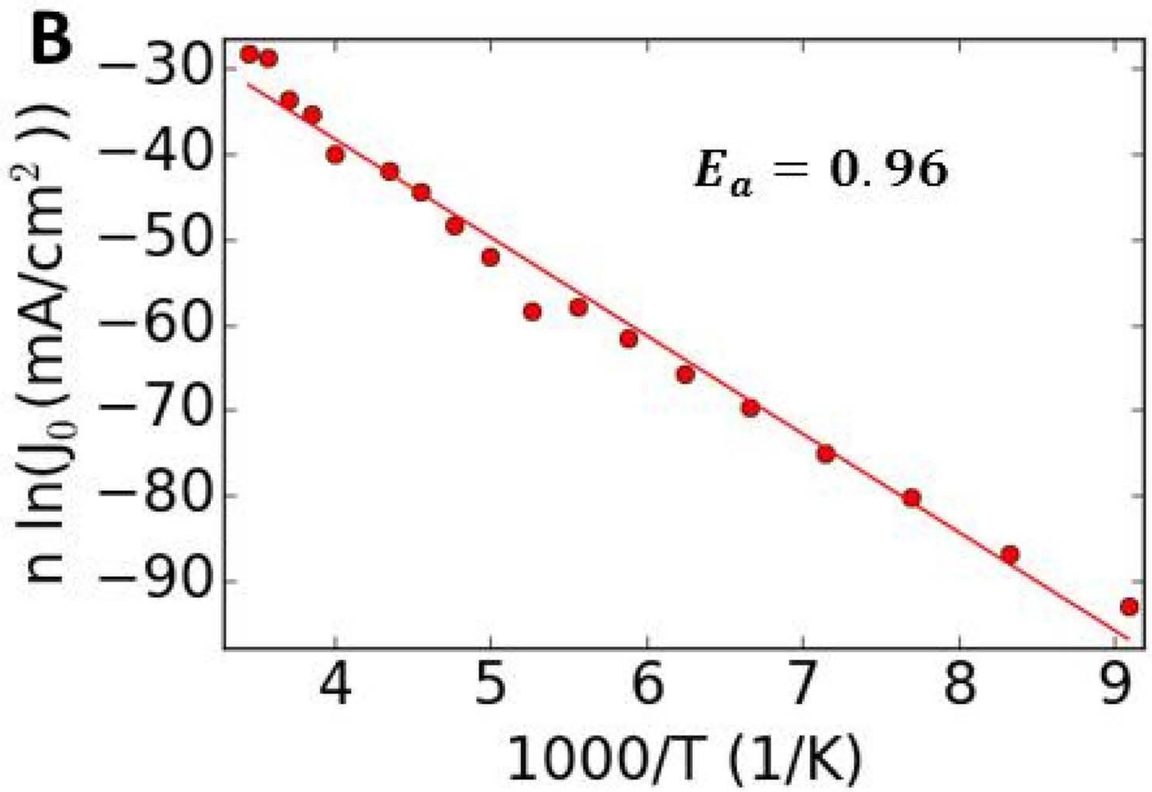
B
n ln(J0 (mA/cm2))
−30
−40
−50
−60
−70
−80
−90
Ea = 0.96
4
5
6
7
8
9
1000/T (1/K)

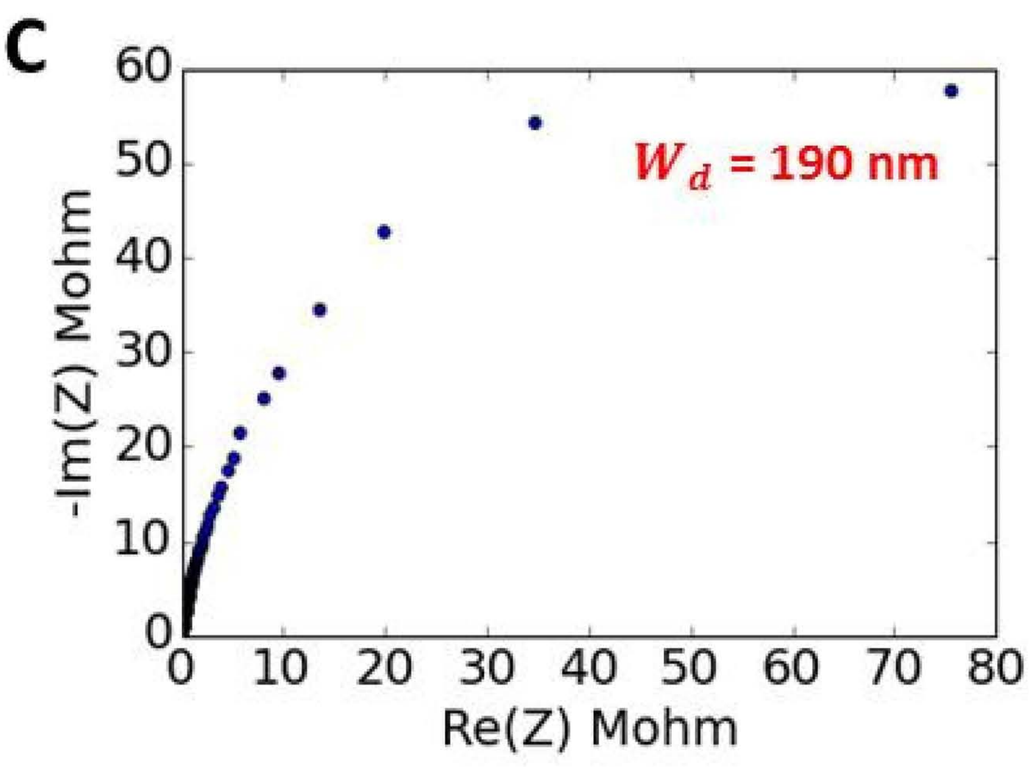
C
-Im(Z) Mohm
60
50
40
30
20
10
0
Wd = 190 nm
0 10 20 30 40 50 60 70 80
Re(Z) Mohm

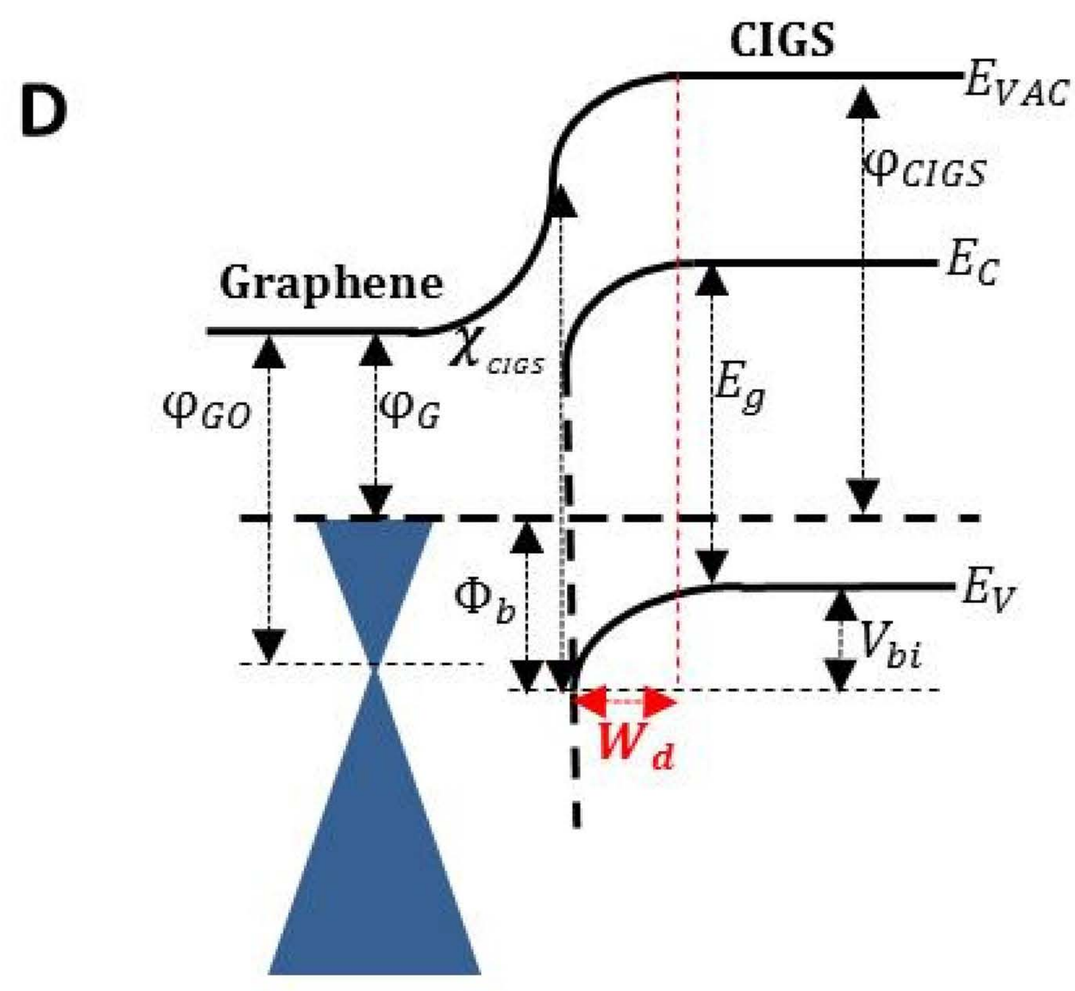
D
CIGS
EVAC
φCIGS
EC
Graphene
χCIGS
φGO
φG
Eg
Φb
EV
Vbi
Wd